Web-Post Buckling Behaviour of Composite Beams with Large Elliptically-Based Web Openings

Eduardo Vedovetto Santos[a], Felipe Piana Vendramell Ferreira[a], Konstantinos Daniel Tsavdaridis[b], Carlos Humberto Martins[a], R. Mark Lawson[c]

[a]Department of Civil Engineering, State University of Maringá, Maringá, Paraná, Brazil.

[b]Department of Engineering, School of Science & Technology, City St George's, University of London, Northampton Square, EC1V 0HB, London, UK.

[c]The Steel Construction Institute, Silwood Park, SL5 7QN, Ascot, UK.

Abstract

Steel beams with elliptically-based web openings have shown higher global shear resistance and increased flexural stiffness compared to those with circular web openings. However, the structural behaviour of steel-concrete composite beams with elliptically-based web openings has yet to be explored. This paper aims to investigate the web-post buckling resistance of steel-concrete composite beams with elliptically-based web openings since this failure mode has become more critical than the Vierendeel mechanism is such perforated beams. A high-fidelity finite element model was developed and a parametric study with 270 models was conducted based on key geometric parameters and various loading conditions. The influence of the geometric parameters of the elliptically-based web opening was examined, and the resistances were presented on bare steel (non-composite) perforated beams in line with previous findings. A previously developed model for predicting the web-post buckling resistance was assessed. The use of the buckling curve 'c', as specified by SCI P355 (2011), provided more effective this study showed that buckling curve 'a' offers better accuracy for calculating the web-post buckling resistance in composite beams with elliptically-based web openings.

Keywords: Composite beams; Elliptically-based web openings; Web-post buckling; Finite element analysis; Eurocode.

E-mails: eduardo.vedovetto@ifpr.edu.br (E. V. Santos); fpvferreira@uem.br; fpiana@live.com (F. P. V. Ferreira); konstantinos.tsavdaridis@city.ac.uk (K. D. Tsavdaridis); chmartins@uem.br (C. H. Martins); m.lawson@steel-sci.com (R. M. Lawson)

1. Introduction

The demand for more efficient structures in Europe has driven the development of methods to improve the performance of lightweight members without adding weight [1]. Advances in automated laser cutting and welding have enabled the production of steel perforated beams with multiple web openings of various sizes, shapes, eccentricities with high precision, hence they are increasingly manufactured. These beams offer solutions for projects requiring open spaces, such as car parks, industrial buildings, offices, and hospitals, and while modernising older structures [2]. Their advantages include longer spans, fewer columns, and integrated building services [3,4]. However, web openings make these beams susceptible to shear as well as buckling, including lateral-torsional buckling (LTB), web-distortion (WD), web-post buckling (WPB), and their interactions [5–8]. Perforated beams with elliptically-based web openings offer an advantage over commonly used circular web openings by allowing the beam to be deeper after its profile (ribbon) cutting manufacturing process, hence further increasing its stiffness, and enhances its WPB resistance due to its web-post plate shape when compared with the cellular beams (perforated beams with periodically spaced circular web openings).

Tsavdaridis and D'Mello [9] tested three steel beam variations with elliptically-based web openings, all of which designed to fail in WPB. The study found that this shape improved stress distribution, while the plastic hinges (stress concentration areas in the vicinity of the web openings) were always formed nearer the neutral axis at the intersection between the semi-circle and the straight lines of the opening's elliptically-based shape. This phenomenon delayed the Vierendeel Mechanism (VM) and increased resistance to global shear stresses compared to beams with circular web openings. Further, Tsavdaridis and D'Mello [1] conducted a comprehensive optimisation study of steel beams with elliptically-based web openings, demonstrating that they offer greater flexural stiffness and additional reduced deflections

compared to beams of similar weights with circular openings. Vertical elliptical web openings allow for more openings along the same beam length while maintaining spacing, reducing weight and embodied CO_2 emissions according to SC4 Ltd[1]. Research studies have shown that deflection can be decreased by approximately 4.5% for spans of 6 to 12 meters.

Later, Ferreira et al. [3] studied the WPB resistance of non-composite steel beams with elliptically-based web openings and proposed a design method. This model is based on the compressed strut approach, and in accordance with BS EN 1993-1-1 [10] guidelines. In this context, SCI P355 [11] recommended the use of buckling curves 'b' and 'c' for hot-rolled and welded sections, respectively. It is worth noting that the recently released BS EN 1993-1-13 [12] guidelines for beams large web openings recommend the buckling curve 'a' to take account the beneficial restraining effects of plate action of the web-post rather than the action of a notional strut. Although these recommendations are targeted at steel beams with circular web openings, they can be applied to steel beams with elliptically-based web openings, as both are manufactured by the same process, considering thermal cutting and welding. However, considering laterally restrained cellular beams, Degtyarev et al. [13] concluded that using EN 1993-1-1 buckling curve 'a', as specified in BS EN 1993-1-13 [12], provided more accurate WPB resistance predictions than curve 'c' required by SCI P355 [11]. However, reliability analyses suggested revising BS EN 1993-1-13 [12] to mandate the use of buckling curve 'c' for WPB resistance predictions.

Shamass et al. [14] recently developed an Artificial Neural Network (ANN) model to predict the WPB resistance of steel beams with elliptically-based web openings. Ferreira et al. [15]

[1] sc4.co.uk

extended the WPB resistance equation to include high-strength steels, while Rabi et al. [3] explored machine learning approaches for predicting the WPB resistance in high-strength steel beams with elliptically-based web openings. Yet, there are no studies of steel-concrete composite beams with elliptically-based web openings in the literature.

Several recommendations have been proposed to predict the WPB resistance of steel beams with web openings. Steel Design Guide 31 [16] and SCI P355 [11] are highlighted, considering the specifications of ANSI/AISC 360-16 [17] and Eurocodes EC3/EC4 [18,19], respectively. However, these publications are addressing steel beams with circular, elongated and hexagonal web openings, and do not consider elliptically-based web openings. It is important to highlight that the failure modes, and consequently the verifications, as well as the resistance calculations, of steel beams with web openings (i.e., castellated, circular, elongated, sinusoidal and elliptically-based) are similar, such as global bending resistance, shear resistance, Vierendeel bending, and resistance to web-post shear, bending and buckling shear resistance, according to BS EN 1993-1-13 [12].

The present study aims to assess the WPB resistance of steel-concrete composite beams with elliptically-based web openings using the finite element method (FEM). WPB is a localised phenomenon which occurs by a lateral displacement coupled with torsion caused by horizontal shear forces acting at the web-post [20]. Geometrically and materially nonlinear analysis with imperfections (GMNIA) was considered. The FE method was developed in two steps: validation and parametric studies. In the validation study, the tests A1 and B1 from Nadjai et al. [21] and 1A and 3 from Müller et al. [22] were considered. After the validation, the parametric study was conducted using models A1, B1, and 1A as reference. This ensured the preservation of the geometric and physical properties, as well as the boundary conditions, maintaining the fidelity of the tested models. In the parametric study, key parameters of the

elliptically-based web openings were varied. A total of 270 FEMs were processed. The results were discussed with a focus on WPB. A comparative analysis was performed and an proposed model for predicting the web-post buckling resistance was assessed. The use of the buckling curve 'a', as specified by FprEN 1993-1-13 [12] is compared with buckling curve 'c' recommended by SCI P355 [11].

2. WPB resistance of steel beams with elliptically-based web openings

The proposed model, which was developed by Ferreira et al. [3], is based on a compressed strut model, as shown in Fig. 1. The procedure consists of determining the effective length ($l_{eff} = k\sqrt{\left(\frac{d_0-2R}{2}\right)^2 + \left(\frac{s}{2} - R\right)^2}$), where k is calculated according to Eq. (1) [3], d_o is the opening height, R is the opening radius, *and* s is the web-post width. After calculating the effective length, the web-post slenderness ($\lambda_w = \frac{l_{eff}\sqrt{12}}{t_w}$) and the critical shear stress in the web-post ($f_{cr,w} = \frac{\pi^2 E}{\lambda_w{}^2}$) are then calculated, in which t_w is the web thickness and E is the Young's Modulus. After calculating these parameters, the BS EN 1993-1-1 [10] methodology is employed, using the concept of relative slenderness ($\lambda_0 = \sqrt{\frac{f_y}{f_{cr,w}}}$), the imperfection ($\phi = 0.5\left[1 + 0.49(\lambda_0 - 0.2) + \lambda_0{}^2\right]$), considering the buckling curve 'c', and the reduction factor ($\chi = \frac{1}{\phi + \sqrt{\phi^2 - \lambda_0{}^2}} \leq 1{,}0$). Finally, the global shear force is calculated, according to Eqs. (2-3) [3].

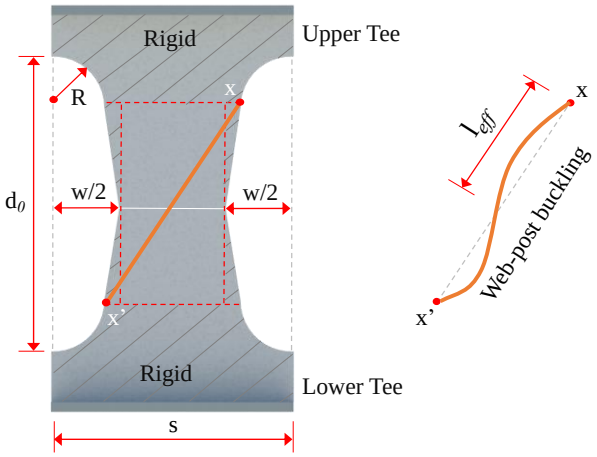

Fig. 1: Compressed strut model for a web-post.

$$k = 0.516 - 0.288\left(\frac{H}{d_0}\right) + 0.062\left(\frac{s}{\mathrm{s-w}}\right) + 2.384\left(\frac{s}{d_0}\right) - 2.906\left(\frac{w}{d_0}\right) \quad (1)$$

$$K = -1.318 + 1.790\left(\frac{H}{d_0}\right) + 0.413\left(\frac{s}{\mathrm{s-w}}\right) - 1.926\left(\frac{s}{d_0}\right) + 0.937\left(\frac{w}{d_0}\right) - 0.02\left(\frac{d_0}{t_w}\right) + 1.412\lambda_0 \quad (2)$$

$$V_{Rk} = K\chi t_w(s-w)f_y \quad (3)$$

3. FE study

Four simply supported composite cellular beams are considered in this study; A1 and B1 from Nadjai et al. [21], and RWTH 1A and RWTH 3 from Müller et al. [22]. These beams are referred here as CCB1, CCB2, CCB3, and CCB4, respectively. The steel deck was omitted to streamline the modelling process [23–25].

3.1. Analysis

The validation of the FE models was conducted in two steps: buckling and post-buckling analyses, both performed using ABAQUS [26]. Buckling analysis, a linear perturbation method, estimates the critical load by multiplying the first buckling mode (positive eigenvalue) by the initial external load, though it does not account for structural imperfections. Therefore, it provides an approximation of critical loads and can aid in incorporating geometric imperfections into nonlinear analyses. For post-buckling analysis, the "Static Riks" method was applied. This method effectively resolves instability problems by accommodating decreases in load or displacement during response. It uses an initial arc length, representing a percentage of the external load or displacement, which ABAQUS [26] adjusts automatically to ensure convergence. Nonlinear equations are solved using the Newton-Raphson method.

3.2. Imperfection

An initial geometric imperfection of $d_g/500$ is used, in which d_g is the total depth of the steel cross-section, as proposed by Shamass et al. [27], Panedpojaman et al. [28] and Lawson at al. [29]. These studies highlight the challenges in estimating imperfections in steel beams with large web openings due to the complexities of the castellation manufacturing process. The implementation of initial geometric imperfection was made by the *IMPERFECTION command, considering the first eigenmode [24]. The residual stresses were not considered, since they do not influence the capacity of composite beams subjected to positive moment [25]. In contrast to the negative moment, the concrete slab in these models contributes to compressive strength. As a result, residual stresses do not affect buckling phenomena associated with flexural behaviour.

3.3. Materials

The material strength values of steel cellular beams are summarised in Table 1. For CCB1, CCB2, CCB3 and CCB4 models, the compressive cylinder strength of concrete (f_{ck} + 8 MPa) is equal to 28.6 MPa, 28.6 MPa, 50.0 MPa and 38.2 MPa, respectively. The constitutive models for steel and concrete used in the numerical modelling are detailed below.

Table 1: Materials strength values (in MPa).

Model	**Ref.**	**Upper Tee**		**Lower Tee**		**f_{ck} (MPa)**
		f_y (flange/web)	**f_u (flange/web)**	**f_y (flange/web)**	**f_u (flange/web)**	
CCB1	[21]	312	438.5	312	438.5	30
CCB2	[21]	312	438.5	312	438.5	30
CCB3	[22]	451/489	541/587	451/489	541/587	42
CCB4	[22]	407/467	524/588	453/488	519/582	30

3.3.1. Steel

The Young's Modulus and the Poisson's ratio are taken equal 200 GPa and a of 0.3, respectively. The quadrilinear steel model by Yun and Gardner [30] (Fig. 2a), according to Eqs. (4-8), is adopted. Regarding shear connectors, the yield stress and the ultimate stress are 460 MPa and 559 MPa, respectively, and the elongation at rupture was 18.8%, in accordance with [31], as shown in Fig. 2b.

$$f(\varepsilon) = \begin{cases} E \cdot \varepsilon, & \varepsilon \le \varepsilon_y \\ f_y, & \varepsilon_y < \varepsilon \le \varepsilon_{sh} \\ f_y + E_{sh}(\varepsilon - \varepsilon_{sh}), & \varepsilon_{sh} < \varepsilon \le C_1\varepsilon_u \\ f_{C_1\varepsilon_u} + \dfrac{f_u - f_{C_1\varepsilon_u}}{\varepsilon_u - C_1 \cdot \varepsilon_u}(\varepsilon - C_1 \cdot \varepsilon_u), & C_1\varepsilon_u < \varepsilon \le \varepsilon_u \end{cases} \quad (4)$$

$$\varepsilon_{sh} = 0.1\frac{f_y}{f_u} - 0.055 \quad (5)$$

$$\varepsilon_u = 0.6\left(1 - \frac{f_y}{f_u}\right) \tag{6}$$

$$E_{sh} = \frac{f_u - f_y}{0.4(\varepsilon_u - \varepsilon_{sh})} \tag{7}$$

$$C_1 = \frac{\varepsilon_{sh} + 0.25(\varepsilon_u - \varepsilon_{sh})}{\varepsilon_u} \tag{8}$$

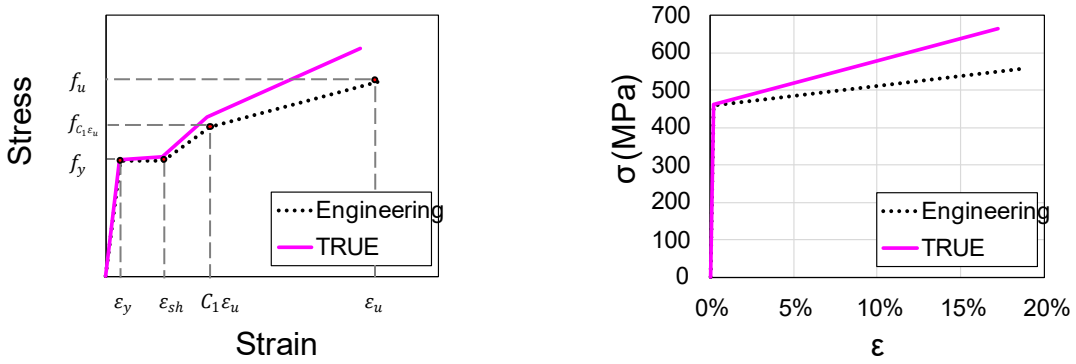

(a) Cellular beams (b) Shear connector

Fig. 2: Stress-strain relationship of steel models

The stress-strain relationships of the steel must be implemented using true values of stress and plastic strain, according to Eqs (9-10), respectively. Steel plasticity model uses the Mises yield surface with associated plastic flow to define the isotropic yielding. Yielding is independent of the equivalent pressure stress and is determined by the uniaxial yield stress as a function of the equivalent plastic strain [26].

$$\sigma_{True} = \sigma_{Eng}(1 + \varepsilon_{Eng}) \tag{9}$$

$$\varepsilon_{True}^{pl} = ln(1 + \varepsilon_{Eng}) - \frac{\sigma_{True}}{E} \tag{10}$$

3.3.2. Concrete

The concrete damage plasticity (CDP) model [32–34] is used, incorporating the compression model from Model Code 2010 [35] (Fig. 3a), and the tension model by Cornelissen et al. [36] (Fig. 3b). Key plasticity parameters were set as dilation angle (40°), eccentricity (0.1), the ratio of initial equibiaxial compressive yield stress to initial uniaxial compressive yield stress (1.16), the ratio of the second stress invariant on the tensile meridian to that on the compressive meridian (0.667), and viscosity parameter (0.001) [23].

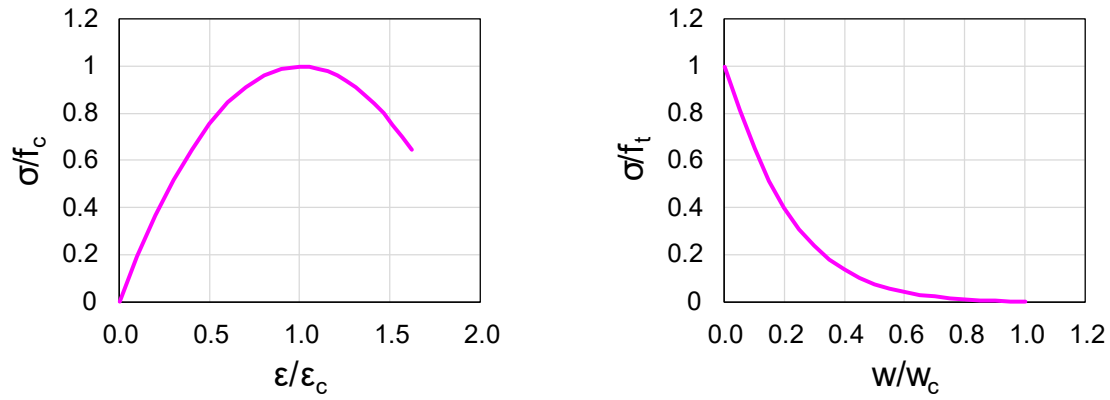

(a) Concrete in compression (b) Concrete in tension

Fig. 3: Stress-strain relationship of concrete models

3.4. Interaction between contact surfaces

A tie constraint was applied to the surface between the shear connectors and the upper flange of the steel profile [37]. This modelling technique simulates a perfect bond between the contact surfaces. For the surfaces between the perforated beam and concrete slab, as well as the concrete slab and shear connectors, normal and tangential contact behaviours were used. Specifically, Coulomb friction coefficients of 0.3 and 0.2 were applied for the perforated beam and concrete slab, and the concrete slab and shear connectors, respectively [38].

3.5. Boundary conditions and discretisation

The steel-concrete composite perforated beam models were simplified by modelling only half of the beam, leveraging longitudinal symmetry. Vertical and lateral displacements (U1=U2=0) were restrained at one end, while mid-span symmetry about the longitudinal axis was applied.

Crisfield [39,40] reported that peak loads are often linked to failure in achieving convergence during the iterative solution process. It was also stated that nonlinear static analysis faces challenges with softening materials, like concrete, which may prevent crack formation or collapse initiation due to the lack of a convergent equilibrium. Therefore, displacement control was adopted herein instead of load application.

Fig. 4 illustrates the mesh discretisation, based on references [23–25,37,38,41–45]. The S4R element is a 4-node quadrilateral shell element with reduced integration and large-strain formulation, with six degrees of freedom per node (three translations and three rotations). It uses linear interpolation and a single integration point at the centre to reduce computational cost. The C3D8R is an 8-node solid brick element with reduced integration and hourglass control, with three displacement degrees of freedom. It also uses linear interpolation for displacement description.

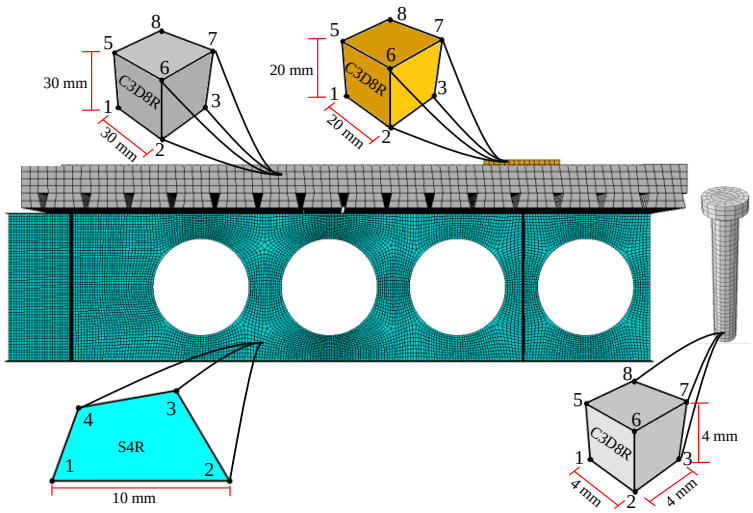

Fig. 4: FE discretisation of the concrete and shear connectors.

3.6. Validation results

The validation results are presented through load-displacement relationships and criteria C1 and C2, as outlined in FprEN 1993-1-14 [46], shown in Fig. 5. The structural resistance is determined from the load and deformation response, considering the lowest resistance based on the two criteria: C1, which corresponds to the maximum load, and C2, which corresponds to a limiting deformation or strain criterion. Note that C2 may occur before reaching the maximum load.

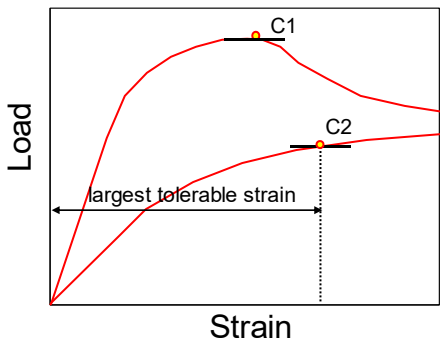

Fig. 5: Criteria C1 and C2, according to FprEN 1993-1-14 [46]

Load versus vertical displacement curves and failure mode shapes from the validation study are shown in Fig. 6. The relative errors between the FE models and tests (P_{FEM}/P_{Test}-1) were -0.3%, -1.8%, -3.7% and 5.2%, for the models CCB1, CCB2, CCB3 and CCB4, respectively. The maximum logarithmic strain in the steel profile was 7.2% for the CCB4 model, while the minimum logarithmic strain was 0.6% for the CCB2 model. On the other hand, regarding the shear connectors, the maximum logarithmic strains in the peak load, were equal to 0.10%, 0.63%, 3.88% and 5.27%, for the models CCB1, CCB2, CCB3 and CCB4, respectively. This means that failure of the shear connector did not occur before WPB. At peak load all deformations remained low. In this way, the criterion used to assess the resistance of the numerical models was the C1.

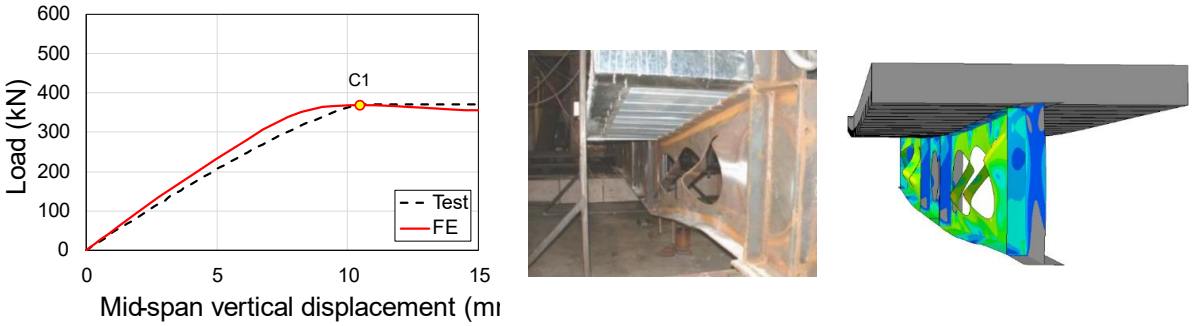

(a) CCB1

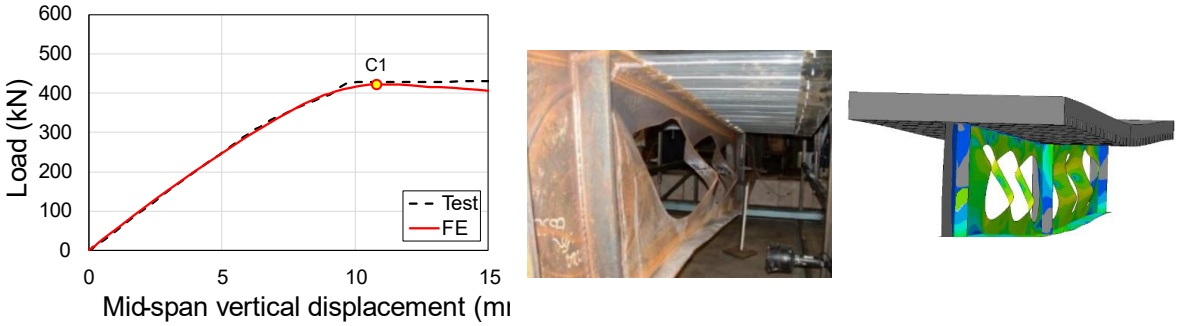

(b) CCB2

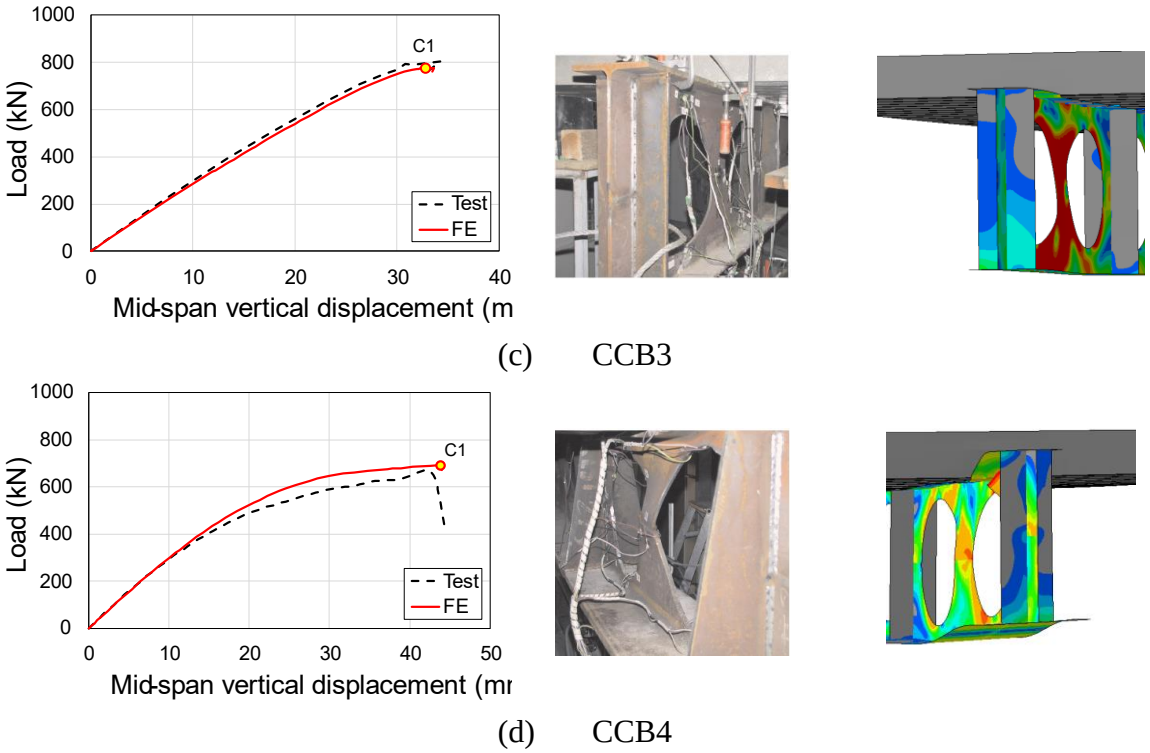

Fig. 6: Validation results of composite cellular beams (Tests from [21] and [22])

The load versus slip relationship of the models was also studied. At peak loads, the observed slips were 0.16 mm, 0.06 mm, 1.22 mm, and 3.49 mm for models CCB1, CCB2, CCB3, and CCB4, respectively. According to the analysis [47] of the CCB1 and CCB2 models tested by [28], the high degree of shear connection ensured full interaction between the slab and beam, preventing slip between steel beams and composite slabs. This was further supported by the absence of shear stud failure before the beam's failure due to WPB. On the other hand, regarding the CCB3 and CCB4 models, Müller et al. [22] stated the unequal slippage on both sides of the composite beams at the failure. However, alike CCB1 and CCB2 models, no shear stud failure occurred as a result of WPB. [20]

3.7. Research significance

In this section, a preliminary study is conducted to evaluate the web-post buckling (WPB) resistance of composite cellular beams against composite beams with elliptical web openings. For this purpose, composite beams with elliptically-based web openings are designed with the same material strengths as those used in the reference models (i.e., CCB1, CCB2, and CCB3). The only variation introduced is the shape of the web openings. To ensure a fair comparison, the Tee section height, the web-post width, and the end-post width are kept constant across all models. Accordingly, the width (w) and height (d_o) of the elliptically-based openings are set equal to the diameter (d_o) of the circular openings. The radius (R) of the semi-circles defining these elliptically-based web openings is defined as $0.4d_o$, ensuring that the area of such web openings closely matches the area of the circular openings.

To carry out this comparison, the same numerical procedure previously developed is applied to ensure consistency and reliability in the analysis. The procedure involves the use of validated computational methods and predefined parameters to assess the behaviour of the composite beams under investigation. The results are illustrated in Fig. 7, which includes both the comparison of the load-displacement relationship and the corresponding deformed configurations at the failure. As shown, composite beams with elliptically-based web openings, when compared to composite cellular beams, demonstrated not only higher initial stiffness but also greater WPB resistance. The resistance ratios of composite beams with elliptically-based web openings to composite cellular beams were 1.23, 1.21, and 1.16 for models CCB1, CCB2, and CCB3, respectively It is important to highlight that the C1 criterion was used to determine the resistance, since the level of deformations remained low, according to the validation study.

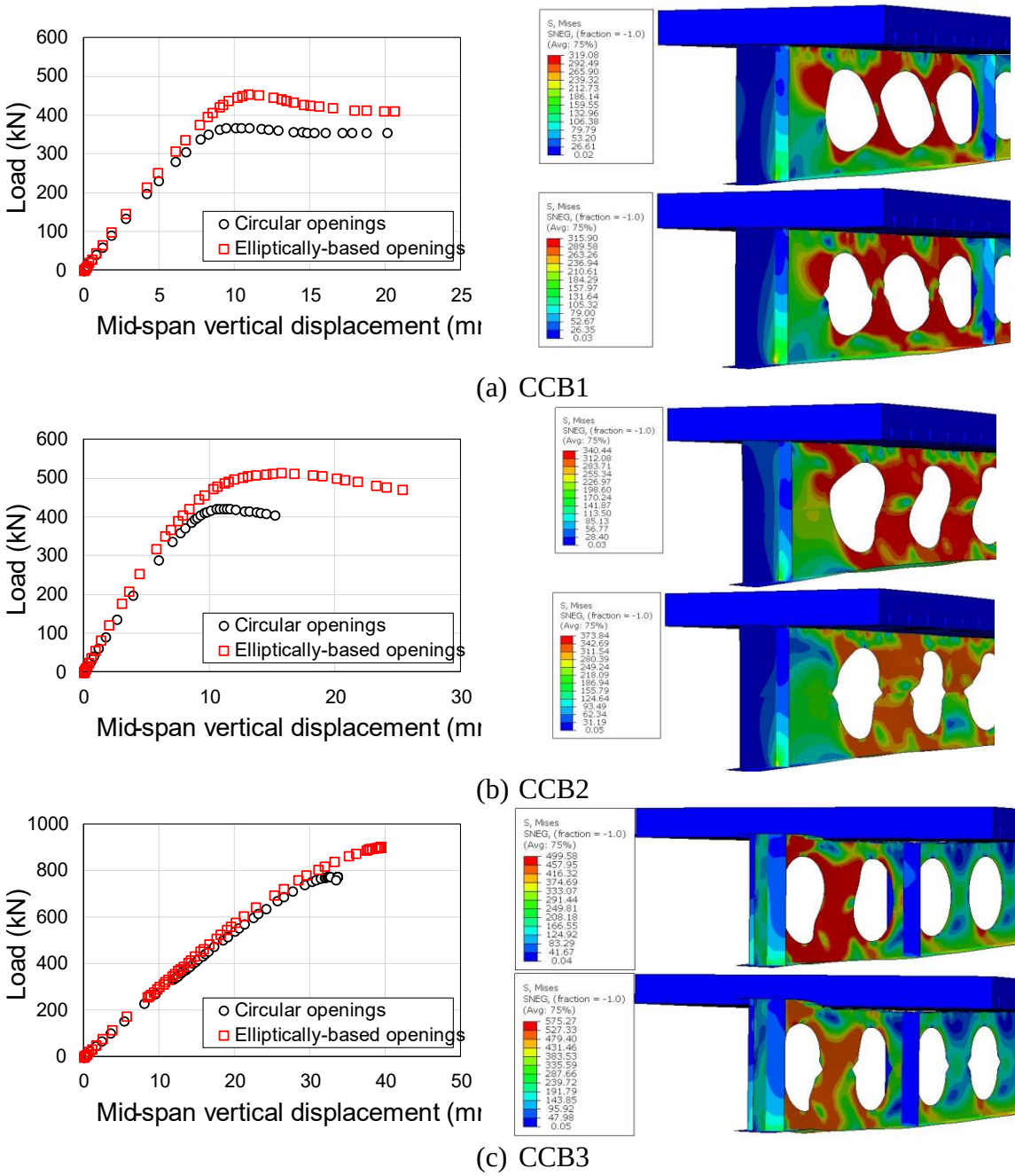

Fig. 7: Preliminary study

The analyses carried out in this section revealed that, for the models under investigation, the composite beams with elliptically-based web openings exhibited, on average, a 20% higher WPB resistance compared to the composite cellular beams. This enhanced performance of the composite beams with elliptically-based web openings can be attributed to their superior structural configuration, which provided increased stability and load-carrying capacity under

the applied conditions. These results highlight the advantages of the composite beams with elliptically-based web openings design in improving resistance to WPB, making it a more effective solution for applications requiring enhanced buckling resistance.

4. Parametric study

Following the preliminary analysis presented in the previous section, it is established that a parametric study of composite beams with elliptically-based web openings that focuses on the variation of geometric parameters of the web openings, is crucial for gaining a deeper understanding of the factors that influence their structural performance and enhancing their efficiency. This approach will allow for the identification of correlations between geometric parameters and the resistance to WPB. The insights obtained from this parametric study can provide the foundation for developing design recommendations and a software, while promoting efficient application of composite beams with elliptically-based web openings in the structural engineering. Thus, the parametric study not only builds upon the findings of the preliminary analysis but also plays a role in advancing both the theoretical understanding and practical implementation of composite beams with elliptically-based web openings.

The parametric study developed is based on the numerical validation studies presented previously, specifically in relation to composite cellular beams. Models CCB1, CCB2, and CCB3 were used as reference models. Thus, the beam span, slab and number of shear connectors were kept constant. The models of parametric study were named for each group as GCCB1, GCCB2, and GCCB3. (Fig. 8), which ‘G’ means ‘Group”. Geometrically and materially nonlinear analysis with imperfections included (GMNIA) were performed for the composite beam models, incorporating a geometric imperfection of $d_g/500$, as outlined in the

validation study. Steel profiles were modelled using S355, according to [30]. The shear connectors were modelled according to the constitutive model presented in Fig. 3a, described previously. Regarding the concrete, the CDP was used, considering the compressive strengths equal to 28.6 MPa, 28.6 MPa and 50 MPa for the models GCCB1, GCCB2, GCCB3, respectively. Stiffeners were considered at load application points and supports, according to the validated models. This study focused on composite beams with elliptically-based web openings subject to web-post buckling, aiming the assessment of the effects of various geometric parameters such as the opening height (d_o), opening radius (R), opening width (w), and web-post width (s-w), as depicted in Fig. 1. The geometric parameters of steel beams with elliptically-based web openings were varied as follows:

- d_o/H: 0.65, 0.70, 0.75, 0.80, 0.85 and 0.90.
- w/d_o: 0.25, 0.35, 0.45, 0.55 and 0.65.
- R/d_o: 0.10, 0.15, 0.20, 0.25 and 0.30.
- b_w/d_o: 0.20, 0.30, 0.40, 0.50 and 0.60 ($b_w = 2R$ in this study, following [3,48]).

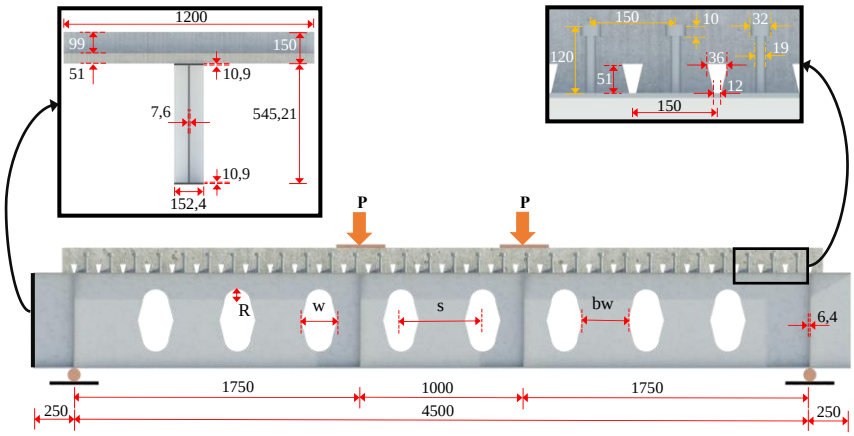

(a) GCCB1

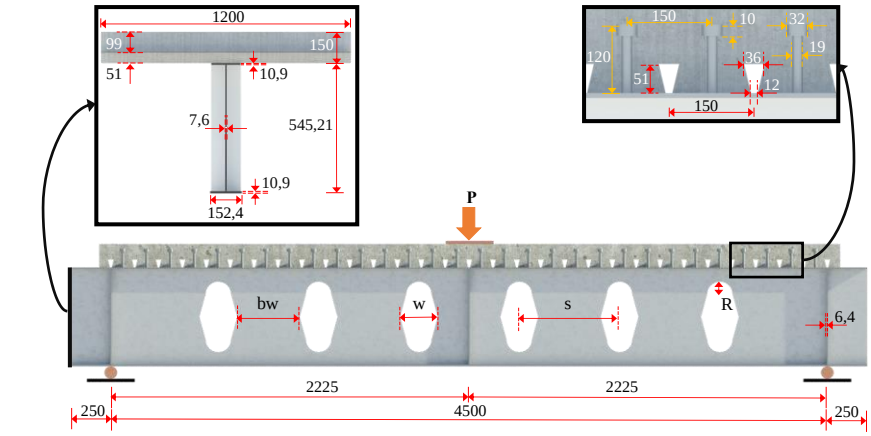

(b) GCCB2

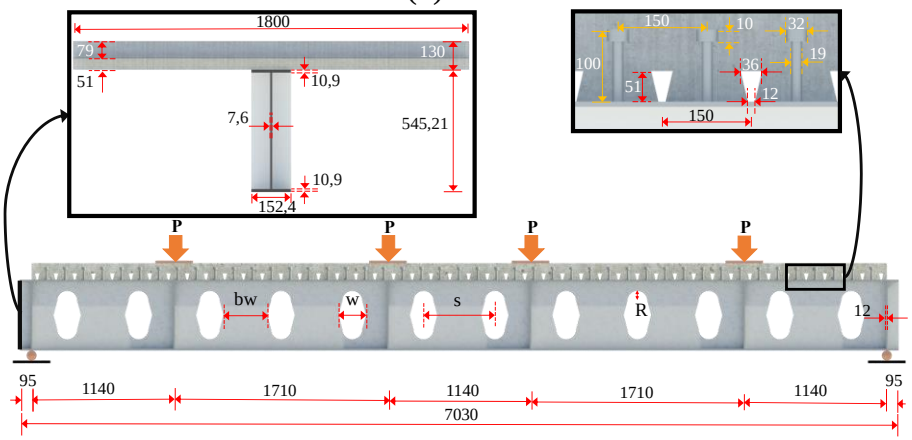

(c) GCCB3

Fig. 8: Parametric study models for composite beams

5. Analysis of parametric study

A total of 270 models were analysed, with 163 models governed by WPB, and the remaining ones by plasticisation caused by VM. The resistance of all models analysed was governed by criterion C1, according to FprEN 1993-1-14 [46] specifications. Table 2 shows the results of the GMNIA, where V1, V2, and V3 represent the global shear forces at the failure for models GCCB1, GCCB2, and GCCB3, respectively. In the next sections, the discussion is focused on the results related to WPB.

Table 2: General results of the GMNIA parametric study

d_o	w	R	b_w	d_o/H	w/d_o	R/d_o	b_w/d_o	V1 (kN)	Failure	V2 (kN)	Failure	V3 (kN)	Failure
350.84	87.71	35.08	70.16	0.65	0.25	0.10	0.20	271.57	WPB	238.56	WPB	111.52	WPB
350.84	122.8	35.08	70.16	0.65	0.35	0.10	0.20	285.64	WPB	267.15	WPB	165.60	WPB
350.84	122.8	52.63	105.26	0.65	0.35	0.15	0.30	294.98	WPB	265.05	WPB	153.45	WPB
350.84	157.88	35.08	70.16	0.65	0.45	0.10	0.20	327.78	WPB	318.40	WPB	174.80	VM
350.84	157.88	52.63	105.26	0.65	0.45	0.15	0.30	316.62	WPB	315.49	WPB	182.78	VM
350.84	157.88	70.17	140.34	0.65	0.45	0.20	0.40	310.44	WPB	305.58	WPB	162.70	VM
350.84	192.96	35.08	70.16	0.65	0.55	0.10	0.20	339.97	WPB	341.83	WPB	135.27	VM
350.84	192.96	52.63	105.26	0.65	0.55	0.15	0.30	345.92	WPB	361.77	WPB	135.56	VM
350.84	192.96	70.17	140.34	0.65	0.55	0.20	0.40	352.48	WPB	378.98	WPB	134.76	VM
350.84	192.96	87.71	175.42	0.65	0.55	0.25	0.50	360.80	WPB	417.71	VM	135.68	VM
350.84	228.05	35.08	70.16	0.65	0.65	0.10	0.20	357.67	WPB	376.40	VM	135.55	VM
350.84	228.05	52.63	105.26	0.65	0.65	0.15	0.30	380.36	WPB	417.07	VM	134.79	VM
350.84	228.05	70.17	140.34	0.65	0.65	0.20	0.40	394.42	WPB	479.91	VM	137.02	VM
350.84	228.05	87.71	175.42	0.65	0.65	0.25	0.50	373.00	WPB	416.86	VM	141.68	VM
350.84	228.05	105.25	210.5	0.65	0.65	0.30	0.60	395.36	WPB	510.40	VM	140.85	VM
377.83	94.46	37.78	75.56	0.70	0.25	0.10	0.20	210.75	WPB	221.88	WPB	147.56	WPB
377.83	132.24	37.78	75.56	0.70	0.35	0.10	0.20	103.60	VM	260.02	WPB	70.29	VM
377.83	132.24	56.67	113.34	0.70	0.35	0.15	0.30	291.31	WPB	263.80	WPB	148.53	VM
377.83	170.02	37.78	75.56	0.70	0.45	0.10	0.20	290.70	WPB	284.27	WPB	165.65	VM
377.83	170.02	56.67	113.34	0.70	0.45	0.15	0.30	315.00	WPB	322.66	WPB	181.45	VM
377.83	170.02	75.57	151.14	0.70	0.45	0.20	0.40	328.95	WPB	325.04	WPB	163.43	VM
377.83	207.81	37.78	75.56	0.70	0.55	0.10	0.20	327.90	WPB	353.61	WPB	190.51	VM
377.83	207.81	56.67	113.34	0.70	0.55	0.15	0.30	341.77	WPB	401.51	WPB	183.36	VM
377.83	207.81	75.57	151.14	0.70	0.55	0.20	0.40	323.34	WPB	334.03	WPB	91.08	VM
377.83	207.81	94.46	188.92	0.70	0.55	0.25	0.50	169.48	VM	356.01	WPB	63.28	VM

377.83	245.59	37.78	75.56	0.70	0.65	0.10	0.20	346.25	WPB	362.38	WPB	193.84	VM
377.83	245.59	56.67	113.34	0.70	0.65	0.15	0.30	167.00	VM	421.61	WPB	210.87	VM
377.83	245.59	75.57	151.14	0.70	0.65	0.20	0.40	401.57	WPB	510.23	WPB	135.18	VM
377.83	245.59	94.46	188.92	0.70	0.65	0.25	0.50	372.45	WPB	91.95	WPB	84.46	VM
377.83	245.59	113.35	226.7	0.70	0.65	0.30	0.60	375.32	WPB	417.05	VM	188.00	VM
404.82	101.21	40.48	80.96	0.75	0.25	0.10	0.20	271.57	WPB	238.56	WPB	111.52	WPB
404.82	141.69	40.48	80.96	0.75	0.35	0.10	0.20	285.64	WPB	267.15	WPB	165.60	WPB
404.82	141.69	60.72	121.44	0.75	0.35	0.15	0.30	294.98	VM	265.05	VM	153.45	VM
404.82	182.17	40.48	80.96	0.75	0.45	0.10	0.20	327.78	WPB	318.40	WPB	174.80	VM
404.82	182.17	60.72	121.44	0.75	0.45	0.15	0.30	316.62	WPB	315.49	WPB	182.78	VM
404.82	182.17	80.96	161.92	0.75	0.45	0.20	0.40	310.44	WPB	305.58	WPB	162.70	VM
404.82	222.65	40.48	80.96	0.75	0.55	0.10	0.20	339.97	WPB	341.83	WPB	135.27	VM
404.82	222.65	60.72	121.44	0.75	0.55	0.15	0.30	345.92	VM	361.77	WPB	135.56	VM
404.82	222.65	80.96	161.92	0.75	0.55	0.20	0.40	352.48	VM	378.98	WPB	134.76	VM
404.82	222.65	101.21	202.42	0.75	0.55	0.25	0.50	360.80	WPB	417.71	WPB	135.68	VM
404.82	263.13	40.48	80.96	0.75	0.65	0.10	0.20	357.67	WPB	376.40	WPB	135.55	VM
404.82	263.13	60.72	121.44	0.75	0.65	0.15	0.30	380.36	WPB	417.07	WPB	134.79	VM
404.82	263.13	80.96	161.92	0.75	0.65	0.20	0.40	394.42	WPB	479.91	WPB	137.02	VM
404.82	263.13	101.21	202.42	0.75	0.65	0.25	0.50	373.00	WPB	416.86	WPB	141.68	VM
404.82	263.13	121.45	242.9	0.75	0.65	0.30	0.60	395.36	WPB	510.40	VM	140.85	VM
431.81	107.95	43.18	86.36	0.80	0.25	0.10	0.20	271.57	VM	238.56	WPB	111.52	WPB
431.81	151.13	43.18	86.36	0.80	0.35	0.10	0.20	285.64	WPB	267.15	WPB	165.60	WPB
431.81	151.13	64.77	129.54	0.80	0.35	0.15	0.30	294.98	WPB	265.05	WPB	153.45	WPB
431.81	194.31	43.18	86.36	0.80	0.45	0.10	0.20	327.78	WPB	318.40	WPB	174.80	VM
431.81	194.31	64.77	129.54	0.80	0.45	0.15	0.30	316.62	WPB	315.49	WPB	182.78	VM
431.81	194.31	86.36	172.72	0.80	0.45	0.20	0.40	310.44	VM	305.58	WPB	162.70	VM
431.81	237.49	43.18	86.36	0.80	0.55	0.10	0.20	339.97	WPB	341.83	WPB	135.27	VM
431.81	237.49	64.77	129.54	0.80	0.55	0.15	0.30	345.92	WPB	361.77	WPB	135.56	VM

431.81	237.49	86.36	172.72	0.80	0.55	0.20	0.40	352.48	WPB	378.98	WPB	134.76	VM
431.81	237.49	107.95	215.9	0.80	0.55	0.25	0.50	360.80	VM	417.71	WPB	135.68	VM
431.81	280.68	43.18	86.36	0.80	0.65	0.10	0.20	357.67	WPB	376.40	WPB	135.55	VM
431.81	280.68	64.77	129.54	0.80	0.65	0.15	0.30	380.36	WPB	417.07	WPB	134.79	VM
431.81	280.68	86.36	172.72	0.80	0.65	0.20	0.40	394.42	WPB	479.91	WPB	137.02	VM
431.81	280.68	107.95	215.9	0.80	0.65	0.25	0.50	373.00	WPB	416.86	WPB	141.68	VM
431.81	280.68	129.54	259.08	0.80	0.65	0.30	0.60	395.36	WPB	510.40	WPB	140.85	VM
458.8	114.7	45.88	91.76	0.85	0.25	0.10	0.20	271.57	WPB	238.56	WPB	111.52	WPB
458.8	160.58	45.88	91.76	0.85	0.35	0.10	0.20	285.64	VM	267.15	VM	165.60	WPB
458.8	160.58	68.82	137.64	0.85	0.35	0.15	0.30	294.98	WPB	265.05	WPB	153.45	WPB
458.8	206.46	45.88	91.76	0.85	0.45	0.10	0.20	327.78	WPB	318.40	WPB	174.80	VM
458.8	206.46	68.82	137.64	0.85	0.45	0.15	0.30	316.62	VM	315.49	VM	182.78	VM
458.8	206.46	91.76	183.52	0.85	0.45	0.20	0.40	310.44	VM	305.58	VM	162.70	VM
458.8	252.34	45.88	91.76	0.85	0.55	0.10	0.20	339.97	WPB	341.83	WPB	135.27	VM
458.8	252.34	68.82	137.64	0.85	0.55	0.15	0.30	345.92	WPB	361.77	WPB	135.56	VM
458.8	252.34	91.76	183.52	0.85	0.55	0.20	0.40	352.48	VM	378.98	WPB	134.76	VM
458.8	252.34	114.7	229.4	0.85	0.55	0.25	0.50	360.80	WPB	417.71	WPB	135.68	VM
458.8	298.22	45.88	91.76	0.85	0.65	0.10	0.20	357.67	VM	376.40	VM	135.55	VM
458.8	298.22	68.82	137.64	0.85	0.65	0.15	0.30	380.36	VM	417.07	VM	134.79	VM
458.8	298.22	91.76	183.52	0.85	0.65	0.20	0.40	394.42	WPB	479.91	WPB	137.02	VM
458.8	298.22	114.7	229.4	0.85	0.65	0.25	0.50	373.00	VM	416.86	VM	141.68	VM
458.8	298.22	137.64	275.28	0.85	0.65	0.30	0.60	395.36	VM	510.40	VM	140.85	VM
485.78	121.45	48.58	97.16	0.90	0.25	0.10	0.20	271.57	WPB	238.56	WPB	111.52	WPB
485.78	170.02	48.58	97.16	0.90	0.35	0.10	0.20	285.64	WPB	267.15	WPB	165.60	WPB
485.78	170.02	72.87	145.74	0.90	0.35	0.15	0.30	294.98	VM	265.05	WPB	153.45	WPB
485.78	218.6	48.58	97.16	0.90	0.45	0.10	0.20	327.78	WPB	318.40	WPB	174.80	WPB
485.78	218.6	72.87	145.74	0.90	0.45	0.15	0.30	316.62	VM	315.49	WPB	182.78	WPB
485.78	218.6	97.16	194.32	0.90	0.45	0.20	0.40	310.44	WPB	305.58	WPB	162.70	WPB

485.78	267.18	48.58	97.16	0.90	0.55	0.10	0.20	339.97	WPB	341.83	WPB	135.27	WPB
485.78	267.18	72.87	145.74	0.90	0.55	0.15	0.30	345.92	WPB	361.77	WPB	135.56	WPB
485.78	267.18	97.16	194.32	0.90	0.55	0.20	0.40	352.48	WPB	378.98	WPB	134.76	VM
485.78	267.18	121.45	242.9	0.90	0.55	0.25	0.50	360.80	WPB	417.71	WPB	135.68	WPB
485.78	315.76	48.58	97.16	0.90	0.65	0.10	0.20	357.67	WPB	376.40	WPB	135.55	VM
485.78	315.76	72.87	145.74	0.90	0.65	0.15	0.30	380.36	WPB	417.07	WPB	134.79	VM
485.78	315.76	97.16	194.32	0.90	0.65	0.20	0.40	394.42	WPB	479.91	WPB	137.02	VM
485.78	315.76	121.45	242.9	0.90	0.65	0.25	0.50	373.00	WPB	416.86	VM	141.68	VM
485.78	315.76	145.74	291.48	0.90	0.65	0.30	0.60	395.36	VM	510.40	VM	140.85	VM

5.1. Buckling analysis

In this section, the buckling modes, considering the first mode, will be discussed as a function of the variation of the geometric parameters of the elliptically-based web openings, as shown in Table 2. In general, the buckling modes exhibited by the GCCB1 models under four-point bending were characterised by WPB near the support (Fig. 9a and Fig. 9b). Also, End-post buckling (EPB) was observed in models where the end distance was significantly greater than the web-post, as shown in Fig. 9c.

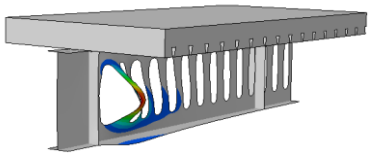

(a) d_o/H = 0.65, w/d_o = 0.25, R/d_o = 0.10

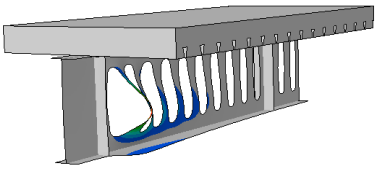

(b) d_o/H = 0.70, w/d_o = 0.25, R/d_o = 0.10

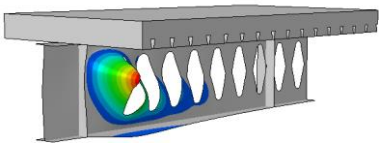

(c) d_o/H = 0.65, w/d_o = 0.45, R/d_o = 0.10

Fig. 9: Buckling modes of GCCB1 models

GCCB2 models were tested under three-point bending. The WPB was verified in most models (Figs. 10a-10b). EPB was also observed in combination with web-post buckling (Fig. 10c). However, as the end distance increased, the EPB as significantly reduced (Fig. 10d).

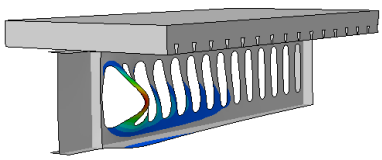

(a) d_o/H = 0.65, w/d_o = 0.25, R/d_o = 0.10

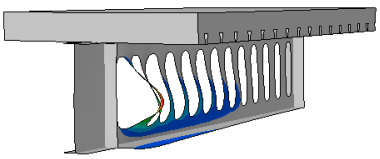

(b) d_o/H = 0.70, w/d_o = 0.25, R/d_o = 0.10

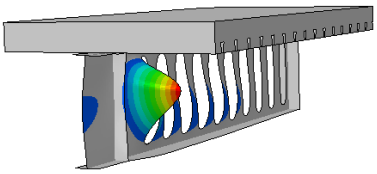

(c) d_o/H = 0.80, w/d_o = 0.25, R/d_o = 0.10

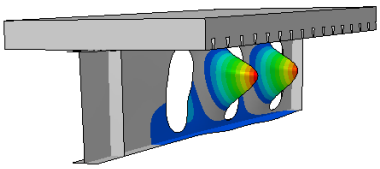

(d) d_o/H = 0.90, w/d_o = 0.65, R/d_o = 0.30

Fig. 10: Buckling modes of GCCB2 models

GCCB3 models were loaded with six-point loading (four loads and two supports). WPB was observed near the supports (Figs. 11a-11b). Due to the increase in the opening height, and consequently the reduction in the Tee section height, the failure of EPB was promoted (Figs. 11c-11d).

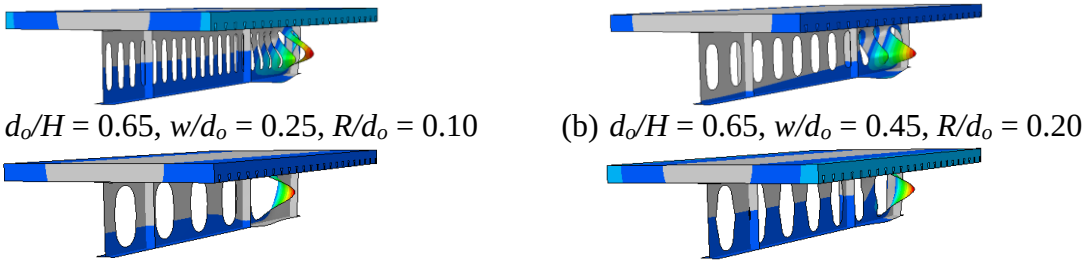

(a) d_o/H = 0.65, w/d_o = 0.25, R/d_o = 0.10 (b) d_o/H = 0.65, w/d_o = 0.45, R/d_o = 0.20

(c) d_o/H = 0.85, w/d_o = 0.65, R/d_o = 0.30 (d) d_o/H = 0.90, w/d_o = 0.55, R/d_o = 0.20

Fig. 11: Buckling modes of GCCB3 models

Another analysis conducted focused on the effective length (l_{eff}), as presented in Section 2. This concept refers to the length of an ideal bar subjected to axial compression and, consequently, buckling. The results presented here, considering composite beams with elliptically-based web openings, were compared with those obtained from web-post models available in [48]. These models represent a simplified numerical analysis approach, specifically aimed at studying WPB. As illustrated in Fig. 12, regarding the web-post models [48], it was observed that as the effective length increased, the critical shear decreased—analogous to a Euler column. However, for composite beams, this relationship was not linear. In other words, unlike the simplified web-post models, interactions between different buckling modes may occur, leading to nonlinear behaviour. Consequently, the effective length is not inversely proportional to the critical shear. The analysis considered the model with d_o/H = 0.65, w/d_o = 0.65, and R/d_o = 0.10-0.30. Notably, as the radius R increased, the effective length also increased.

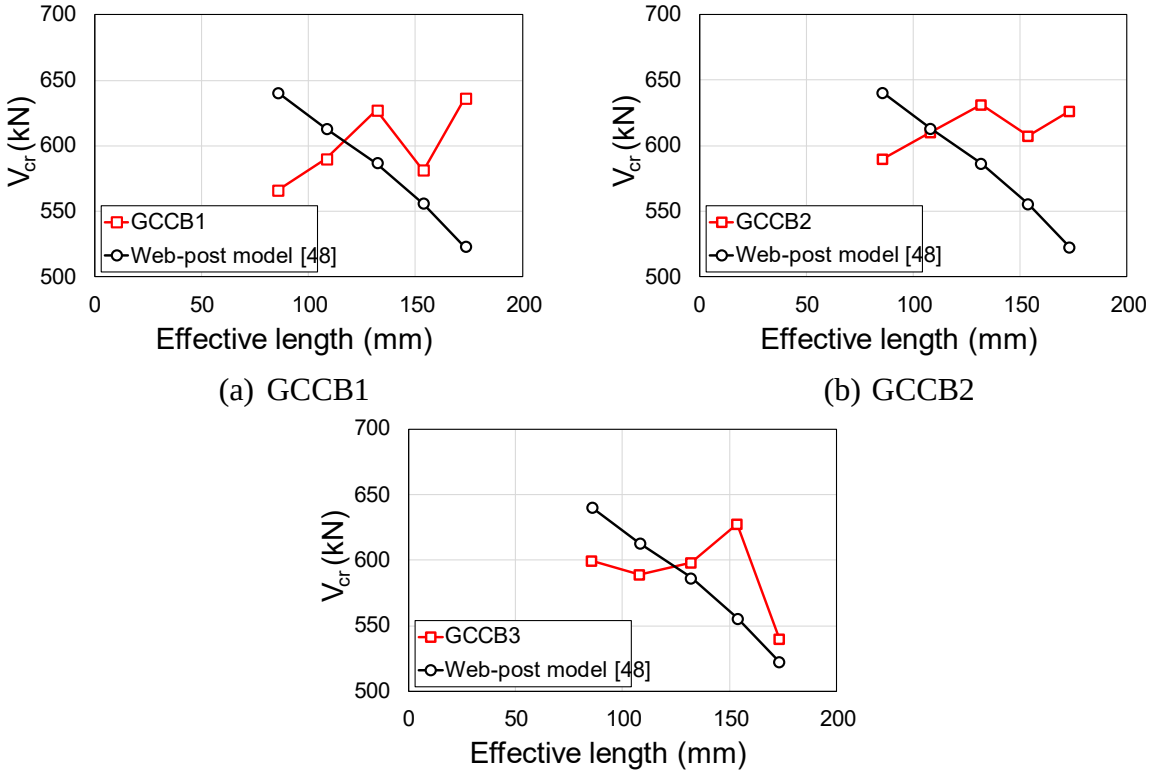

(a) GCCB1 (b) GCCB2

(c) GCCB3

Fig. 12: Comparison between the effective length – web-post models [48] vs. composite beam models.

Fig. 13 below illustrates the interaction of buckling modes in the models analysed for effective length. For models GCCB1-3, an interaction was observed between local buckling at the top tee and WPB. As the radius *R* increased, an additional interaction was identified, involving these modes along with local buckling of the bottom flange.

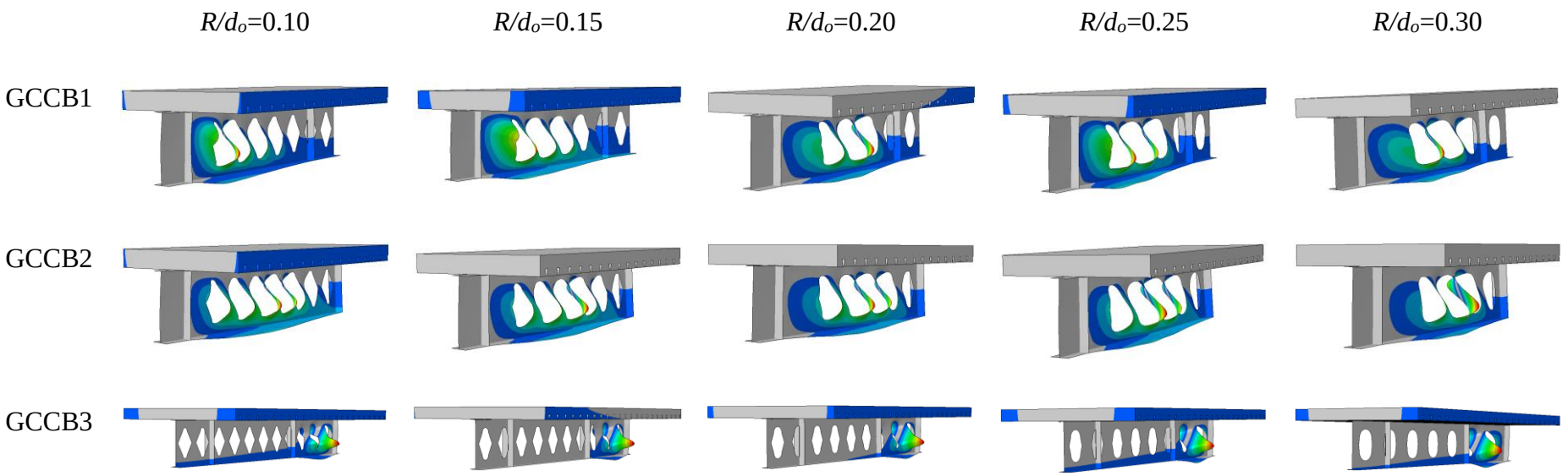

Fig. 13: Buckling modes of the effective length analyses as function of R/d_o

5.2. Post-buckling analysis

5.2.1. *GCCB1*

The failure mode for the reference section GCCB1 (d_o/H = 0.65) was characterised by WPB, as shown in Fig. 14a–14b. Increasing the web-post width reduced local stress concentrations, particularly in models with w/d_o = 0.65, which corresponded to the largest opening ratios. Models with d_o/H = 0.70 and d_o/H = 0.75 predominantly failed due to WPB (Fig. 14b–14c). In both cases, stresses in the steel profile increased with higher w/d_o, with models having R/d_o = 0.25 showing the highest stresses. For d_o/H = 0.80, a significant number of models failed due to WPB (Fig. 14d). Models with w/d_o = 0.35 and w/d_o = 0.45 exhibited the highest web-post stresses, while those with w/d_o = 0.55 and w/d_o = 0.65 experienced higher stresses near the end-post due to their larger web-post width. Approximately half of the models with d_o/H = 0.85 failed due to WPB, showing the highest stresses in the web-post (Fig. 14e). Considering d_o/H = 0.90, WPB failures were common, with models experiencing the highest stresses overall (Fig. 14f).

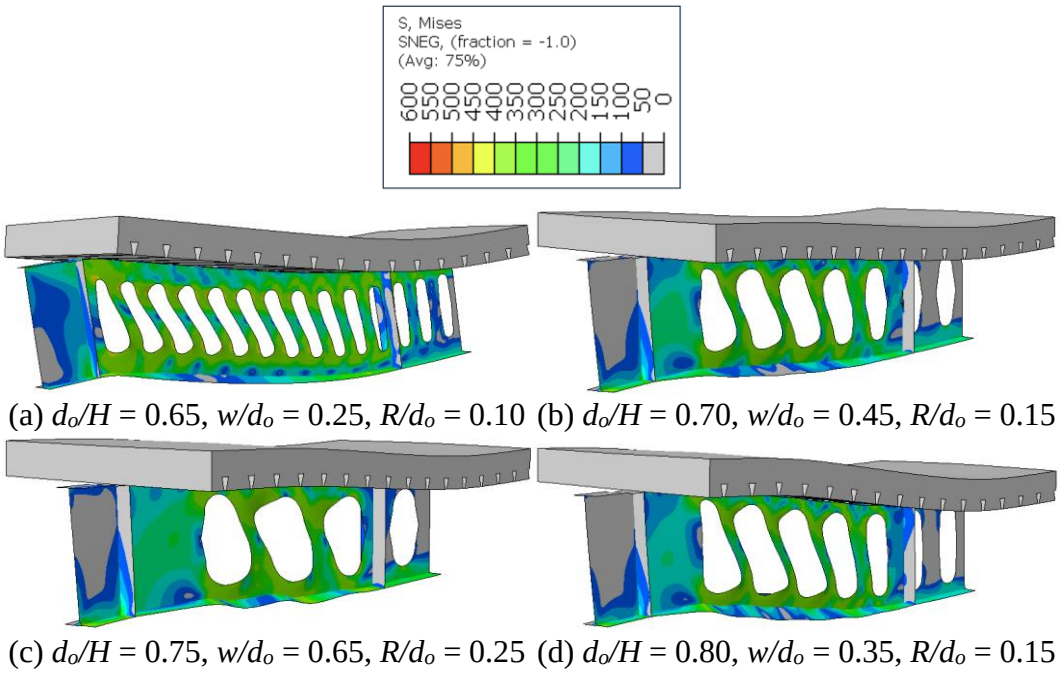

(a) d_o/H = 0.65, w/d_o = 0.25, R/d_o = 0.10 (b) d_o/H = 0.70, w/d_o = 0.45, R/d_o = 0.15

(c) d_o/H = 0.75, w/d_o = 0.65, R/d_o = 0.25 (d) d_o/H = 0.80, w/d_o = 0.35, R/d_o = 0.15

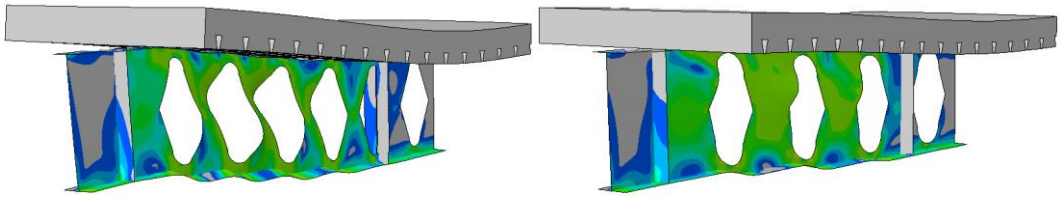

(e) d_o/H = 0.85, w/d_o = 0.55, R/d_o = 0.10 (f) d_o/H = 0.90, w/d_o = 0.65, R/d_o = 0.20

Fig. 14: WPB (Von Mises stresses in MPa), GCCB1.

Another analysis conducted was related to the stress distribution, considering the principal directions of the shell elements in the steel beam with elliptically-based openings. This is because the presence of openings may cause local bending stress concentrations. The stresses presented in the Fig. 15 for the GCCB1 model represent the principal stresses associated with the structural behaviour up to the failure load of the beam. This model was subjected to four-point bending, resulting in a more evenly distributed loading regime along the span. As the load increased, regions reaching the yield stress tended to concentrate in the web-post along the S22 direction, characterising the WPB phenomenon. This effect occurred due to local web flexure between the web openings, indicating that this direction played a significant role in the beam's reduction of load-bearing capacity. In the S11 direction, the GCCB1 model generally exhibited only small regions with stress concentrations at the failure load. These concentrations were mainly located above and below the elliptically-based web openings, suggesting that the geometry of the openings significantly affected the redistribution of longitudinal stresses. The von Mises stresses in the GCCB1 model were highly concentrated around the openings, where the highest stress occurred due to the geometric discontinuity. This can compromise the beam's strength if the ratio between the opening diameter and the web height (do/H) was high, as it may reduce the section's stiffness. The structural behaviour of the GCCB1 model indicated that stress $S22$ was the primary factor driving material nonlinearity and, consequently, the beam's loss of strength. On the other hand, stress $S11$, although influenced by the presence of web openings, had a less significant impact on the overall load-bearing capacity. To optimise the

model, it is recommended to investigate the influence of geometric adjustments, such as increasing the curvature radius at the ends of the openings (R/d_o), to reduce local stress concentrations and improve the beam's structural efficiency under loading.

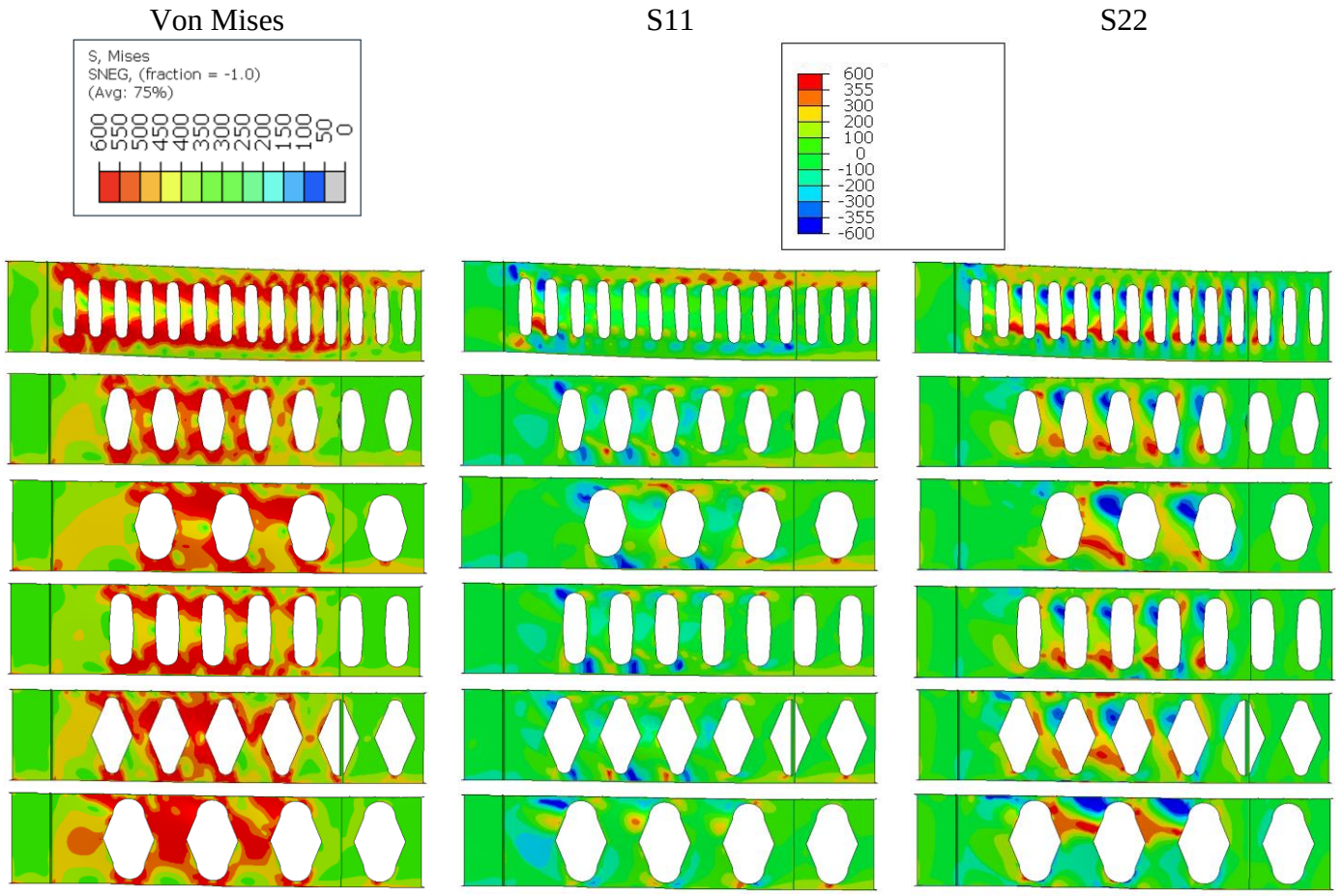

Fig. 15: Stresses in MPa, GCCB1.

The reference model GGCB1 was tested under four-point bending, featuring two regions with constant global shear and one region with constant bending moment (pure bending). Regarding the V/M ratio (global shear to bending moment), the GGCB1 models generally exhibited minimum and maximum values of 0.41 and 8.42, respectively. The highest values were observed near the supports, while the lowest occurred in the mid-span region. This analysis revealed that failure modes associated with shear forces, such as WPB, were identified at the openings close to the supports, whereas modes related to bending, such as plasticisation, occurred near the mid-span.

Fig. 16 shows the analysis of the parameters d_o/H and w/d_o for global shear. The analyses conducted demonstrate that the variation in the w/d_o ratio, compared to the d_o/H ratio, had a significant impact on the variation of stresses associated with the WPB failure mode. This result indicates that, when the opening height (d_o) is kept constant, the opening width (w_o) plays predominant role in determining the resistance to WPB. In practical terms, this suggests that changes in the w_o directly influence the distribution and concentration of stresses in the vicinity of the web-post, making it a crucial factor for improving structural resistance against WPB. On the other hand, variations in d_o had a less significant effect compared to changes in w_o, emphasising the importance of prioritising adjustments in w/d_o ratio during the design or optimisation processes. Variations were observed for some models with d_o/H = 0.7. This variation occurred because these models have a lower end-post width compared to the others for the same R/d_o and w/d_o ratios. Practically, this suggests that changes in the w/d_o ratio during the design or optimisation of structural projects affect the dimensions of the web-post width and, consequently, the end-post width, directly influencing the resistance to buckling.

For elliptically-based web openings, varying the height (d_o), while keeping the radius (R) constant does not significantly affect WPB resistance. This is due to the unchanged width between the web openings – set as $b_w = 2R$ in this study, following [3,48].

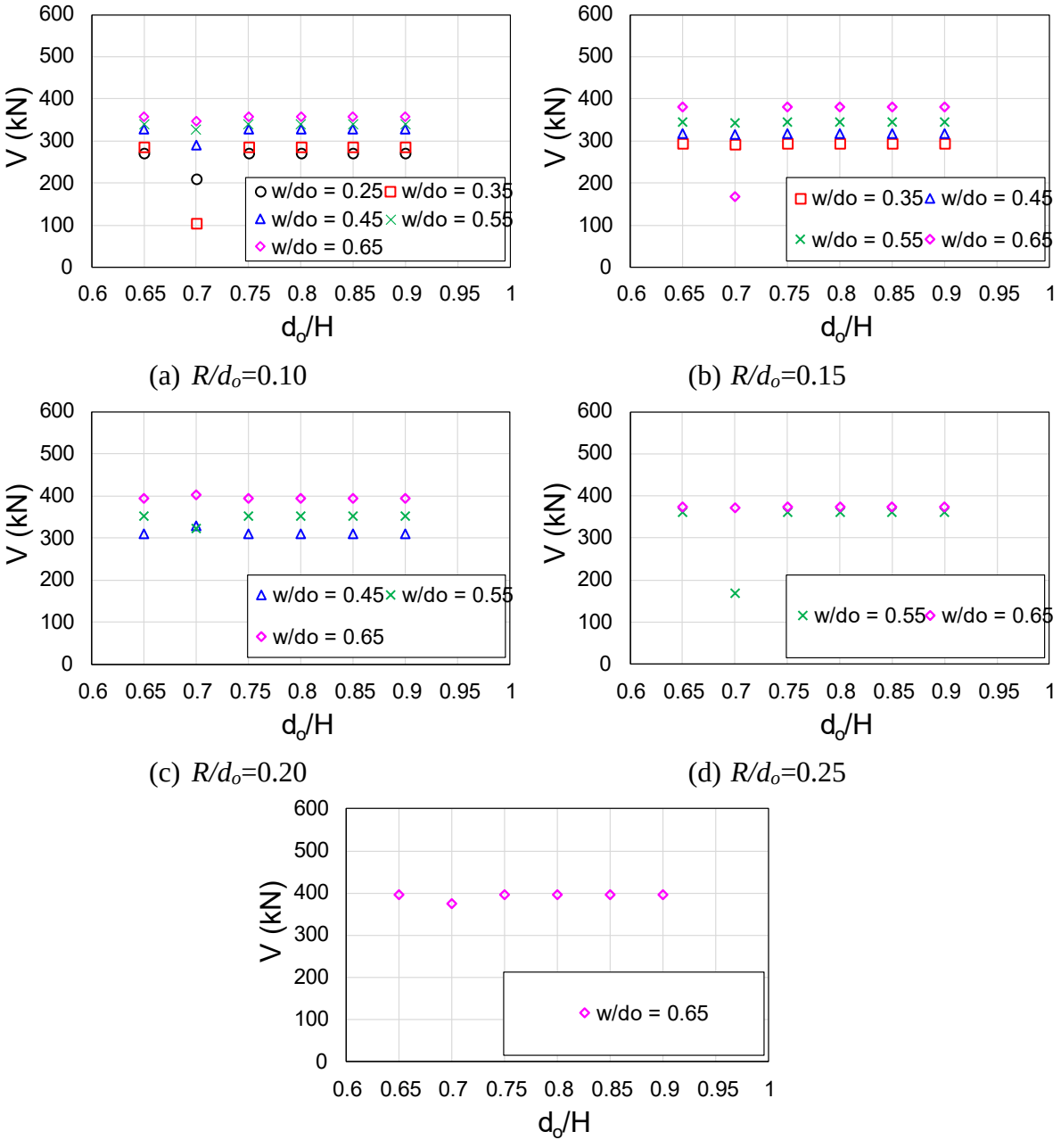

(a) R/d_o=0.10 (b) R/d_o=0.15

(c) R/d_o=0.20 (d) R/d_o=0.25

(e) R/d_o=0.30

Fig. 16: Comparison of parameters for the GCCB1 models.

5.2.2. *GCCB2*

Fig. 17a shows the GCCB2 reference model with d_o/H=0.65. It was evident that increasing the web-post width reduced stress concentrations, shifting stress to the mid-span, with failure caused by plasticisation from VM in the vicinity of the web openings. Regarding GCCB2 reference models with d_o/H=0.70, as shown in Fig. 17b, it can be observed that stresses in the steel profile increased with higher w/d_o, with most failures governed by WPB. For models with d_o/H=0.75, a significant number of failure models were characterised by WPB, according to Fig. 17c. It was also noticeable that stresses were concentrated in the lower region of the central opening, with models at w/d_o = 0.65 showing the highest stresses. Considering models with d_o/H=0.80, as shown in Fig. 17d, higher stresses were observed compared to d_o/H = 0.75, especially for w/d_o of 0.55 and 0.65, attributed to larger opening areas in the web-post. All GCCB2 reference models with d_o/H=0.85 failed due to WPB, as seen in Fig. 17e. These models exhibited higher stress values for small w/d_o compared to the previous d_o/H ratios. For the GCCB2 reference models with d_o/H=0.90, shown in Fig. 17f, it was observed that models with larger web-post openings experienced high stresses and consistently failed due to WPB.

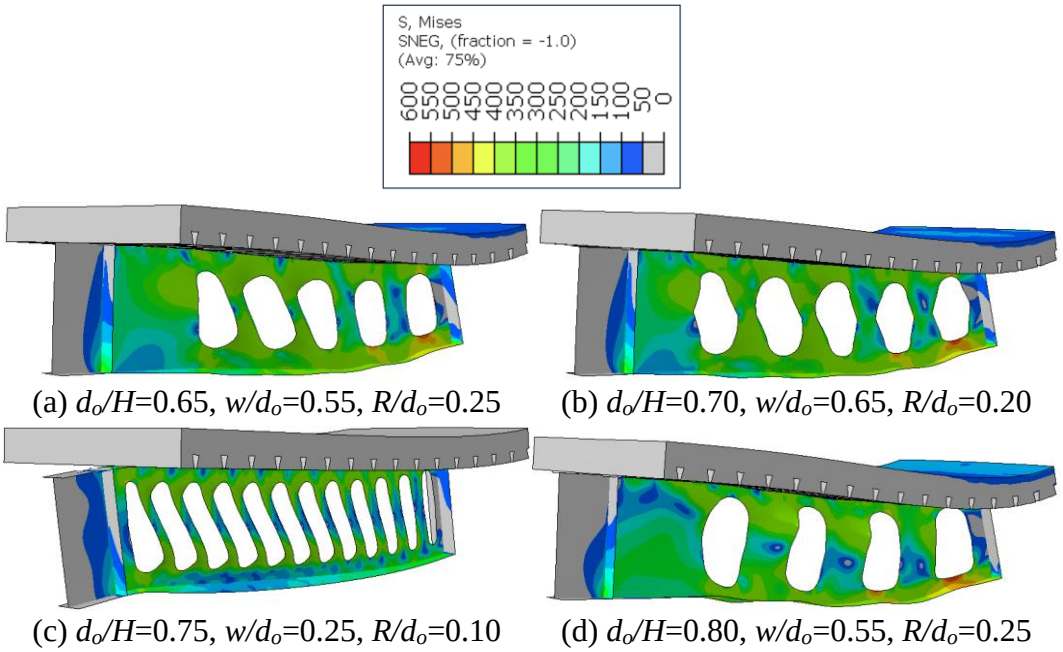

(a) d_o/H=0.65, w/d_o=0.55, R/d_o=0.25 (b) d_o/H=0.70, w/d_o=0.65, R/d_o=0.20

(c) d_o/H=0.75, w/d_o=0.25, R/d_o=0.10 (d) d_o/H=0.80, w/d_o=0.55, R/d_o=0.25

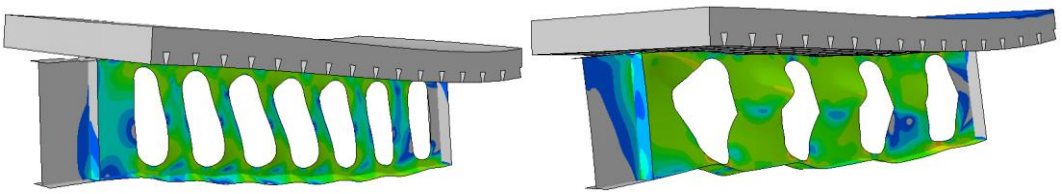

(e) d_o/H=0.85, w/d_o=0.35, R/d_o=0.15 (f) d_o/H=0.90, w/d_o=0.65, R/d_o=0.20

Fig. 17: WPB (Von Mises stresses in MPa) for model GCCB2.

Fig. 18 illustrates the stress distribution (S11 and S22) in the GCCB2 model, which was subjected to three-point bending, resulting in a higher concentration of stresses in the central region of the beam. The von Mises stresses were increased around the elliptically-based web openings, especially below the load application point. S22 stress exhibited high concentrations in the web posts, characterising WPB, while S11 stress shows localised concentrations above and below the web openings, though with a lesser structural impact. The severity of the three-point bending load increased the likelihood of localised plasticisation, making the opening geometry a critical factor for structural resistance.

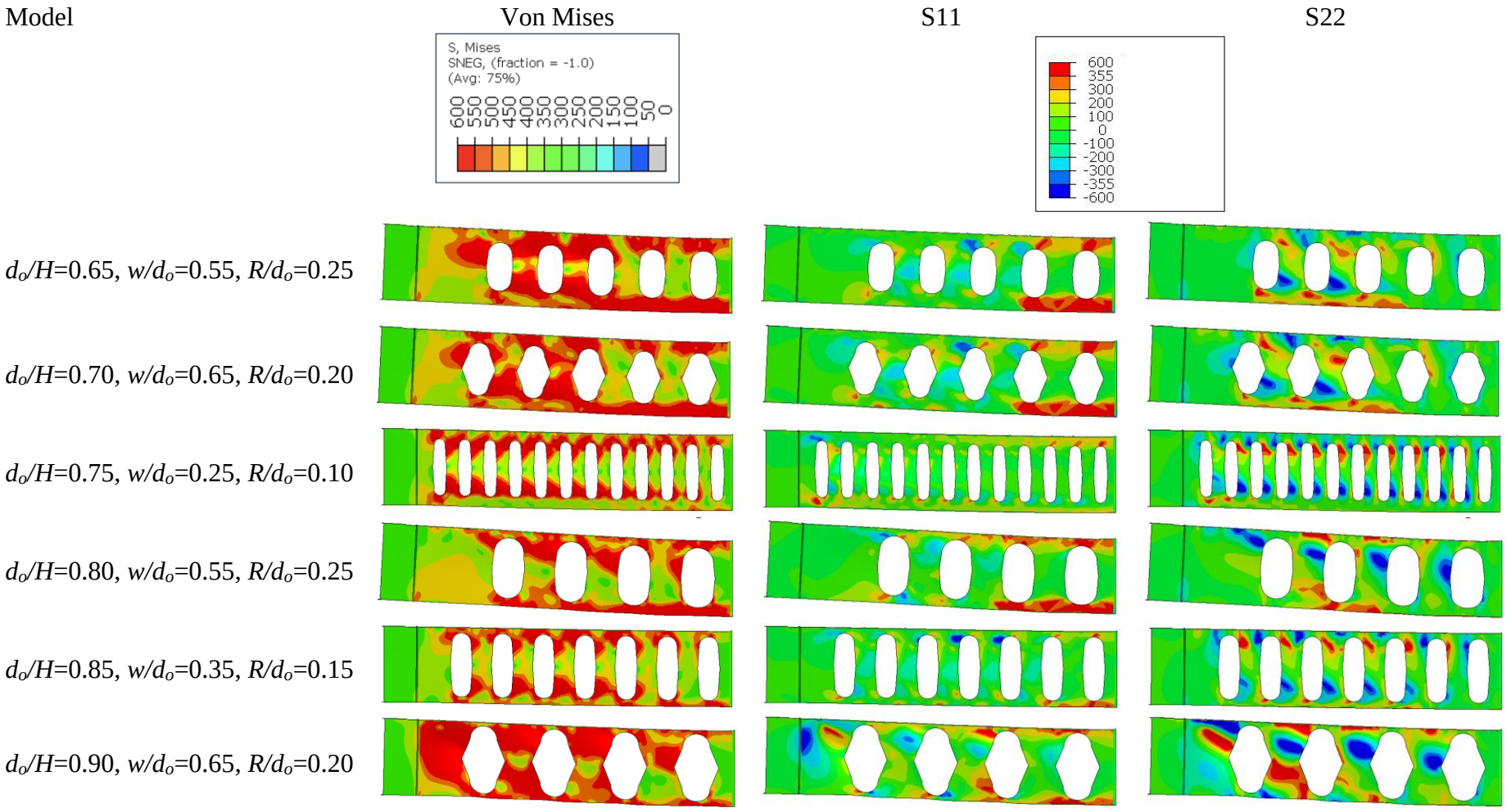

Fig. 18: Stresses in MPa, GCCB2.

Unlike the reference model GGCB1, the reference model GGCB2 was subjected to three-point bending, featuring two regions with constant shear and no region with constant bending moment (only variable). Regarding the V/M ratio, the GGCB2 models exhibited minimum and maximum values of 0.39 and 8.42, respectively. Similar to the GGCB1 model, the high V/M ratio values observed in the analysed models indicated that the predominant failure mode was WPB.

Observing ratios d_o/H and w/d_o for global shear in the GCBB2 finite element models (Figs. 19a-19e), it was noticeable that for any w/d_o, as the d_o/H increases, this caused a greater variation in global shear. It was also observed that models with higher w/d_o exhibited greater global shear, possibly due to their larger web-post widths. Similar to the GCCB1 model, variations were observed in some models with do/H = 0.7, due to the end-post width being smaller compared to the other models for the same R/d_o and w/d_o ratios.

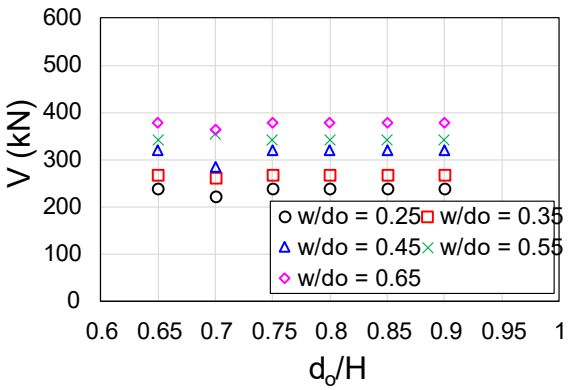

(a) R/d_o=0.10

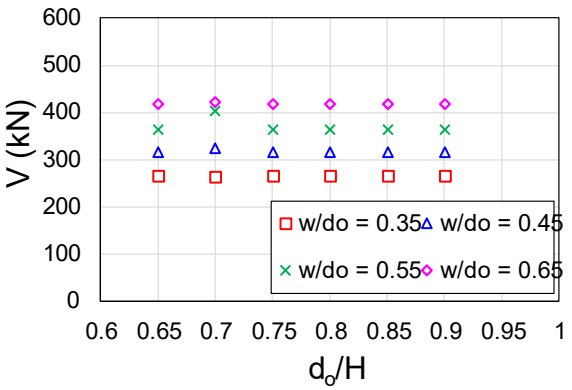

(b) R/d_o=0.15

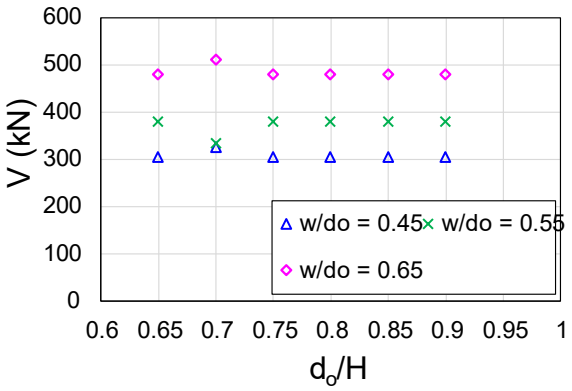

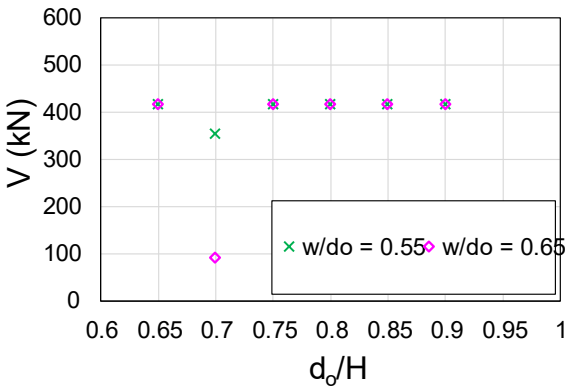

(c) R/d_o=0.20 (d) R/d_o=0.25

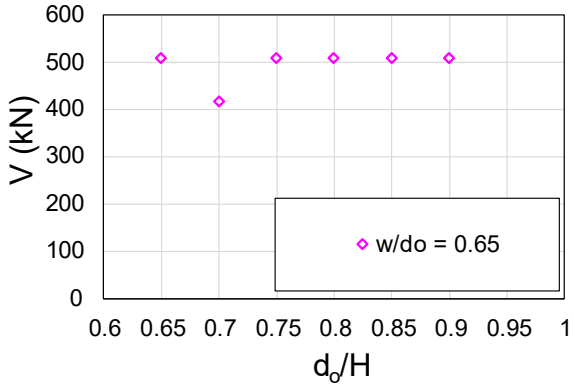

(e) R/d_o=0.30

178 Fig. 19: Comparison of parameters for the GCCB2 models.

179 Like GCCB1 models, for GCCB2 models, the interaction between d_o/H and w/d_o also plays a
180 critical role in influencing both the localised stress distribution and the overall structural
181 behaviours of the models, particularly concerning global shear and failure by WPB. Models
182 with wider web-post, higher w/d_o ratios, and greater d_o/H ratios are more susceptible to WPB
183 failure. This increased likelihood of failure is attributed to the elevated stress concentrations
184 that occur around the web openings and along the regions adjacent to the larger openings.

185 Larger w/d_o ratios intensify the stresses on the web-post by increasing the web-post width
186 relative to the opening height. This amplifies the stresses in critical regions, particularly near
187 the central and edge openings, making the web-post more vulnerable to buckling. Similarly,
188 higher d_o/H ratios, which correspond to higher openings, exacerbate stress magnitudes and
189 redistribution, further diminishing structural stability under loading.

190 Adjustments to the web-post width can significantly influence the WPB resistance. By
191 optimising w/d_o, it is possible to reduce stress concentrations, enhance load redistribution, and
192 mitigate the risk of WPB. This demonstrates the importance of a balanced design approach that
193 considers both d_o/H and w/d_o to improve structural performance and resistance to WPB,
194 ensuring the models maintain their integrity under varying load conditions.

5.2.3. *GCCB3*

The failure modes observed for models with d_o/H=0.65 were characterised by WPB considering models with w/d_o ratios of 0.25 and 0.35. It was noticeable that increasing the web-post width tends to reduce stress concentrations. This situation was particularly evident for models with a w/d_o ratio of 0.65, where the highest opening ratio and the widest web-post were observed. However, von Mises stresses are higher for models with smaller web-post widths. In Fig. 20a, it was observed that for models with smaller w/d_o ratios, failure occurred due to WPB near the support end. For the remaining models, stress concentrations were observed in the lower region of the first two openings at the mid-span, indicating failure mode governed by plasticisation due to VM. For d_o/H=0.70-0.75, the failures predominantly resulted from plasticisation due to VM, with stresses increasing in the lower central region as w/d_o increase, indicating stress transfer to the lower flange. Models with d_o/H=0.80 failed by VM, with peak stresses observed for w/d_o ratios of 0.55 and 0.65, attributed to larger web-post openings (Fig. 20b). This could be due to the increased opening area of the web-post for these models. For models with d_o/H=0.85, the failures remained governed by VM, with the highest stresses occurring at mid-span in the lower region. WPB-induced stress concentrations were also observed in the web-post (Fig. 20c). Considering very height openings with d_o/H=0.90, WPB occurred for w/d_o ratios of 0.25–0.55, while w/d_o = 0.65 led to VM, due to reduced flange height caused by the large openings (Figs. 20d). In other words, the results indicated that increasing the web-post width generally helps to reduce shear-induced stress concentrations within the perforated steel beam. This is particularly evident in models with wider web-post, where the stress concentrations near the openings are diminished. However, as the width and the height of the openings increase, the likelihood of failure shifts towards plasticisation and VM. This shift becomes more pronounced as the ratio of w/d_o increases, suggesting that wider web-posts lead to a reduction

in the flange height, thus contributing to a higher tendency for failure due to bending rather than shear. In higher d_o/H ratios, plasticisation became the predominant failure mode due to the increased bending moments. As the openings increased, stress redistribution occurred, transferring more efforts to the lower flange, which can further intensify the bending-induced failure.

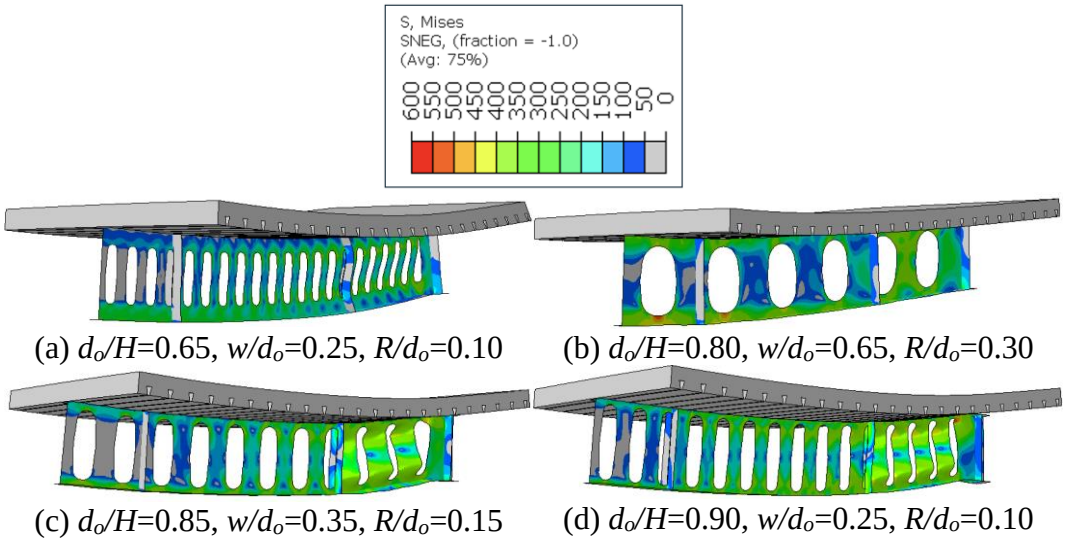

(a) d_o/H=0.65, w/d_o=0.25, R/d_o=0.10 (b) d_o/H=0.80, w/d_o=0.65, R/d_o=0.30

(c) d_o/H=0.85, w/d_o=0.35, R/d_o=0.15 (d) d_o/H=0.90, w/d_o=0.25, R/d_o=0.10

Fig. 20: WPB (Von Mises stresses in MPa) for model GCCB3.

The GCCB3 model, subjected to six-point bending, exhibited a more balanced distribution of stresses along the beam span, reducing stress concentration at a single point and favoring stress redistribution, compared to the GCCB1 model (four-point bending) and GCCB2 model (three-point bending), according to Fig. 21. The distribution of von Mises stresses was more uniform. *S*22 stress, perpendicular to the beam's axis, showed lower concentrations than in the other models, although it still indicates WPB. The longitudinal stress *S*11 was more evenly distributed, with smaller concentration peaks, reducing the risk of localised plasticity. Regarding potential structural failures, the GCCB3 model was more efficient due to reduced stress concentration.

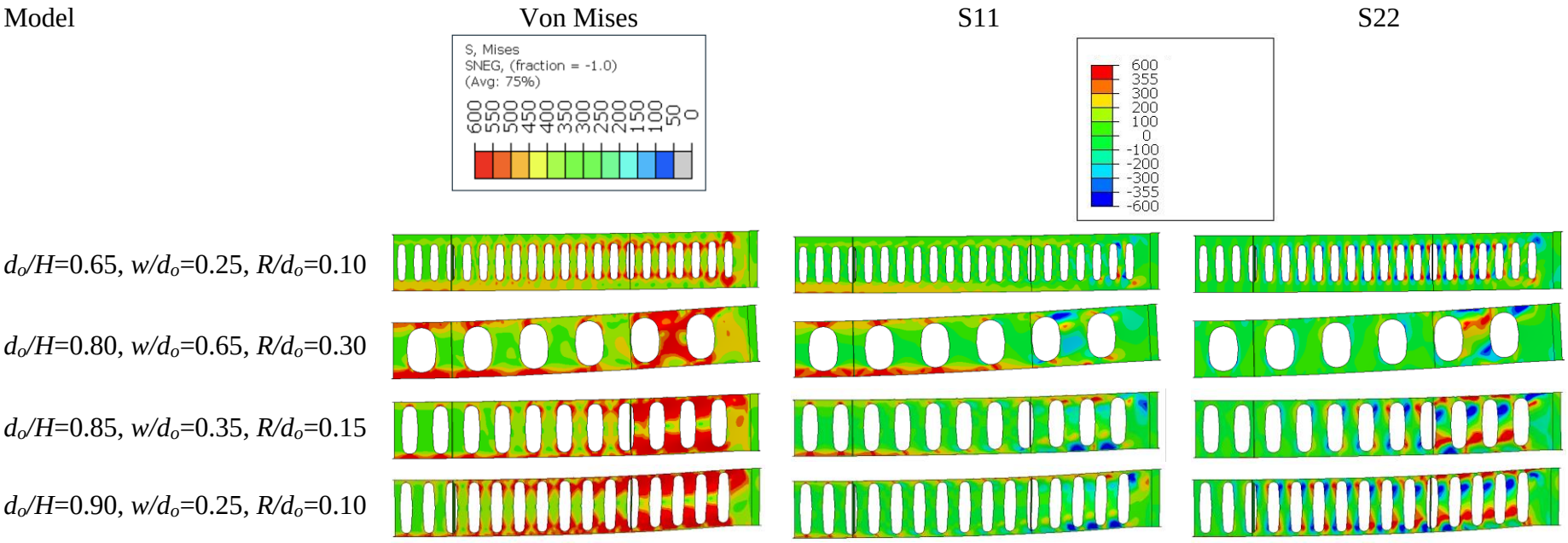

Fig. 21: Stresses in MPa, GCCB3.

240 The GGCB3 model features a longer span compared to the GGCB1 and GGCB2 models.
241 Additionally, the GGCB3 was subjected to six-point bending, with four load application points
242 and two supports. Regarding the V/M ratio, the GGCB3 models exhibited minimum and
243 maximum values of 0.25 and 5.44, respectively. Notably, these values are lower than those
244 observed in the GGCB1 and GGCB2 models. Lower V/M ratio values in the analysed models
245 indicated that the predominant failure mode was associated with plasticisation phenomena. In
246 this context, bending behaviour predominated over shear behaviour.

247 Observing the ratios d_o/H, w/d_o, and R/d_o in the GCCB3 models (Figs. 22a-22e), it was
248 concluded that the w/d_o ratio of 0.45 varies shear force as the opening height and opening radius
249 increase. Models with w/d_o ratio of 0.55 and R/d_o of 0.10 and 0.15 exhibited similar behaviours,
250 similar with w/d_o ratio of 0.65, and R/d_o of 0.20 and 0.25. These models had the highest opening
251 area ratios, suggesting that shear resistance was associated with WPB. It is important to
252 highlight that variations were observed in some models with do/H = 0.7, due to the end-post
253 width being smaller compared to the other models.

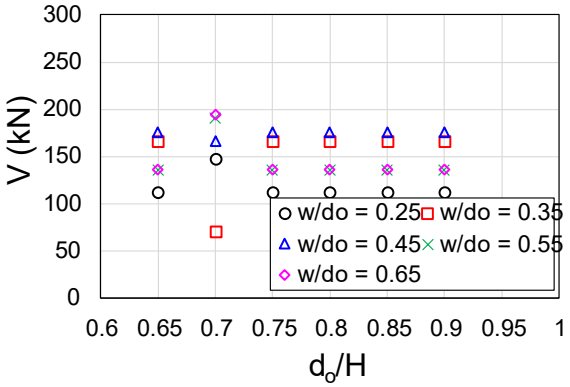

(a) R/d_o=0.10

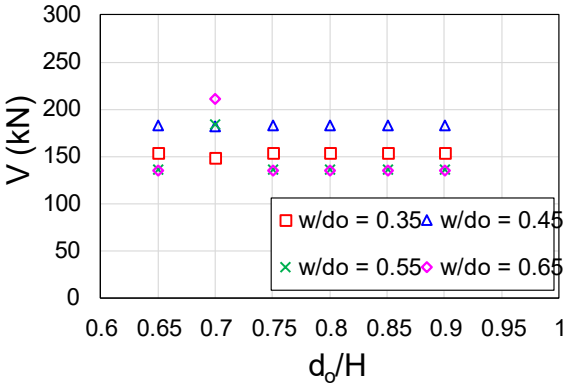

(b) R/d_o=0.15

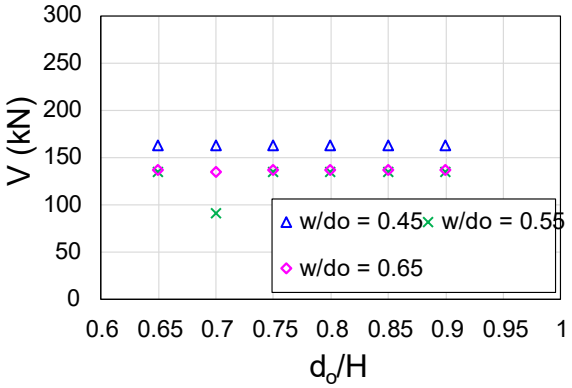

(c) R/d_o=0.20

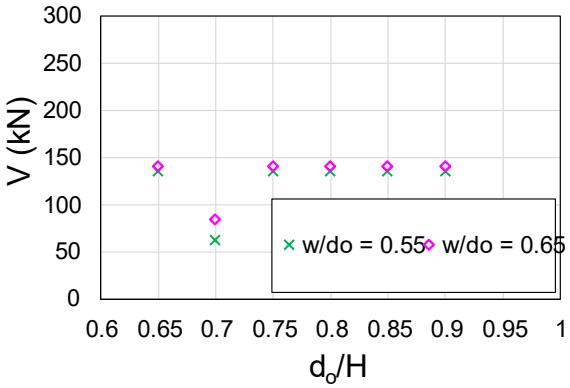

(d) R/d_o=0.25

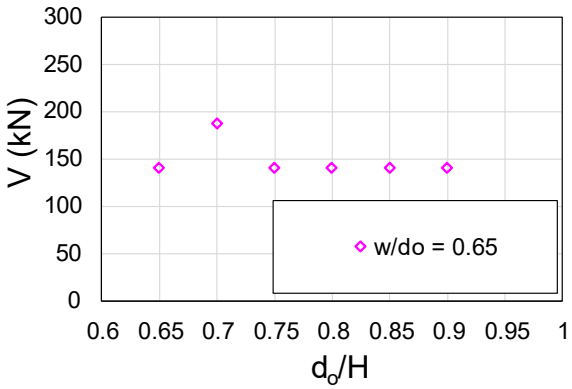

(e) R/d_o=0.30

254 Fig. 22: Comparison of parameters for the GCCB3 models.

255

256 5.3. Comparative analysis

257 To conduct a comparative analysis, the proposed model, which was developed by Ferreira et
258 al. [3], was considered for validation, along with the resistance differences of the GCCB1,
259 GCCB2, and GCCB3 models, as a function of the variation in the geometric parameters of the
260 opening.

261

262

263

5.3.1. FEM vs. Ferreira et al. [3]

Finite element models exhibiting failure modes defined by WPB were utilised in this discussion to compare with the procedure proposed by Ferreira et al. [3] (V_{Rk}). For values of $V_{FEM}/V_{Rk}\geq1.0$, the resistance of the proposed model is more conservative that the finite element model predictions, indicating safety requirements [49] for WPB are met.

For GCCB1 models (Fig. 23a), using curve 'c' as a reference, it was observed that as the opening height increased, the discrepancy between numerical (V_{FEM}) and proposed model (V_{Rk}) also increased. In this context, out of the total number of models, 63 favour safety ($V_{FEM}/V_{Rk}\geq1.0$) and 4 unsafety ($V_{FEM}/V_{Rk}<1.0$). For these models, the mean, the standard deviation, the maximum and minimum relative error (V_{FEM}/V_{Rk}-1) were 1.19, 0.16, 73.4% and -8.7%, respectively. The GCCB2 models, according to Fig 23b, exhibited a response similar to that of the GCCB1 models. It was found that 65 models were in favour of safety ($V_{FEM}/V_{Rk}\geq1.0$), while 7 were unsafety ($V_{FEM}/V_{Rk}<1.0$). The GCCB2 models with a mean, standard deviation, maximum, and minimum relative errors of 1.26, 0.24, 106.7%, and -11.8%, respectively. Regarding the GCCB3 models (Fig. 23c), all models were unsafety ($V_{FEM}/V_{Rk}<1.0$). For these models, the mean and standard deviation were equal to 0.63 and 0.05, respectively. The maximum and minimum relative errors were equal to -28.7% and -48.9%, respectively.

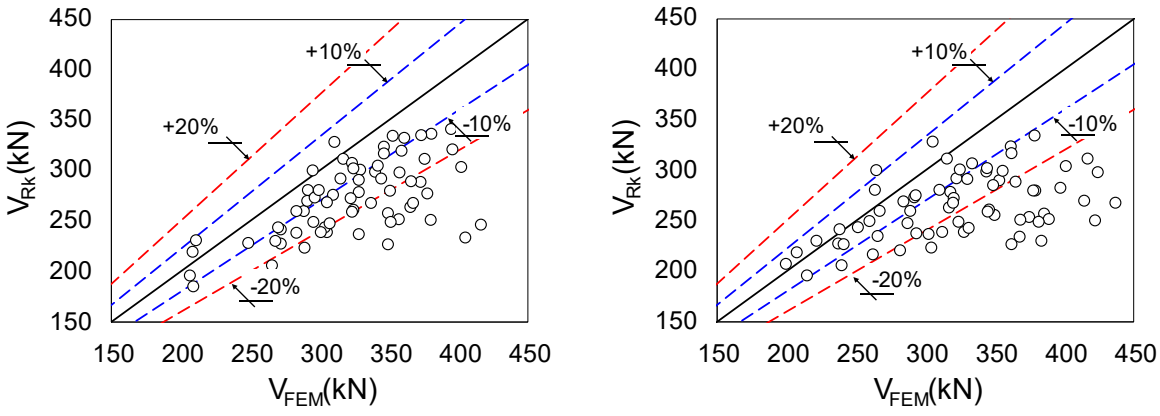

(a) GCCB1 models (b) GCCB2 models

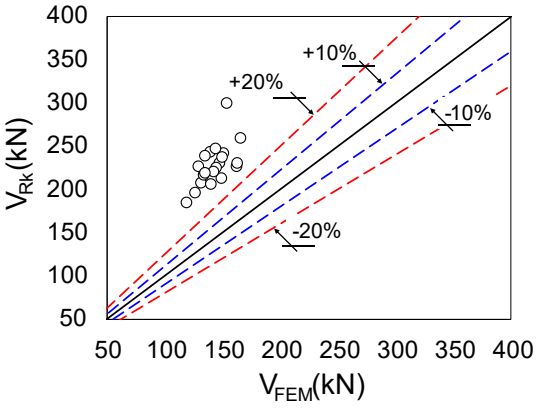

(c) GCCB3 models

281 Fig. 23: Comparison between finite element models and predictions by Ferreira et al. [3],
282 considering buckling curve ‘c’

283

284 Using curve "a" as a reference for the proposed model predictions, the WPB resistance for the
285 GCCB1 models (Fig. 24a) predicted 30 models in favour of safety ($V_{FEM}/V_{Rk}\geq1.0$) and 37
286 against safety ($V_{FEM}/V_{Rk}<1.0$). The mean, standard deviation, maximum, and minimum relative
287 errors were 1.00, 0.13, 48.2%, and -20.3%, respectively.

288 For the GCCB2 models (Fig. 24b), there were 37 models in favour of safety ($V_{FEM}/V_{Rk}\geq1.0$)
289 and 35 against safety ($V_{FEM}/V_{Rk}<1.0$). The mean and standard deviation were 1.06 and 0.19,
290 respectively, while the maximum and minimum relative errors were 76.6% and -22.7%,
291 respectively. Considering now, the GCCB3 models (Fig. 24c), all models were unsafety
292 ($V_{FEM}/V_{Rk}<1.0$). For these models, the mean and standard deviation were equal to 0.53 and 0.04,
293 respectively. The maximum and minimum relative errors were equal to -41.3% and -55.2%,
294 respectively.

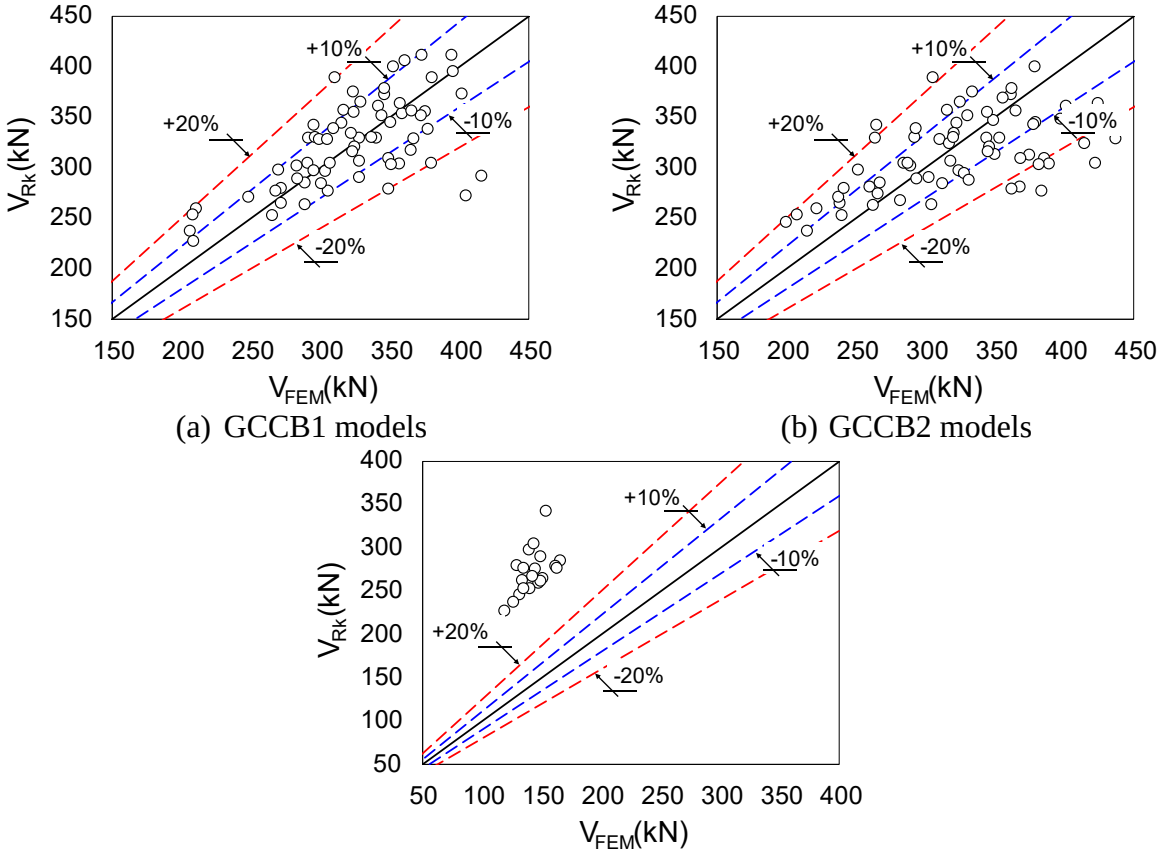

295 Fig. 24: Comparison between finite element models and predictions by Ferreira et al. [3],
296 considering buckling curve 'a'

297 In addition to the comparative analysis based on relative errors, a normal distribution analysis
298 was conducted for all models, as shown in Fig. 25. Notably, the normal distribution of curve
299 '*a*' is shifted to the left compared to curve *c*, with a lower mean value (0.97 vs. 1.15). This
300 indicates that curve '*a*' generally predicts lower values. Both distributions exhibit a similar
301 coefficient of variation, suggesting comparable relative dispersion considering the ratio
302 V_{FEM}/V_{Rk}. However, curve '*c*' has a slightly lower standard deviation (0.23 vs. 0.28) and a
303 broader range (0.51 to 2.07 vs. 0.45 to 1.77), implying greater variability and the presence of
304 more extreme values. These characteristics suggest that curve '*c*' provides more conservative
305 estimates than curve '*a*', making it a potentially safer option in the context of the analysis. These
306 findings align with the SCI P355 [11]. However, the recently published FprEN 1993-1-13 [12]

307 recommends using buckling curve '*a'* for large web openings. This recommendation considers
308 the beneficial restraining effects of the web-post's plate action rather than the action of a
309 notional strut. Although all these guidelines are intended for steel beams with circular web
310 openings, they can also be applied to steel beams with elliptically-based web openings.

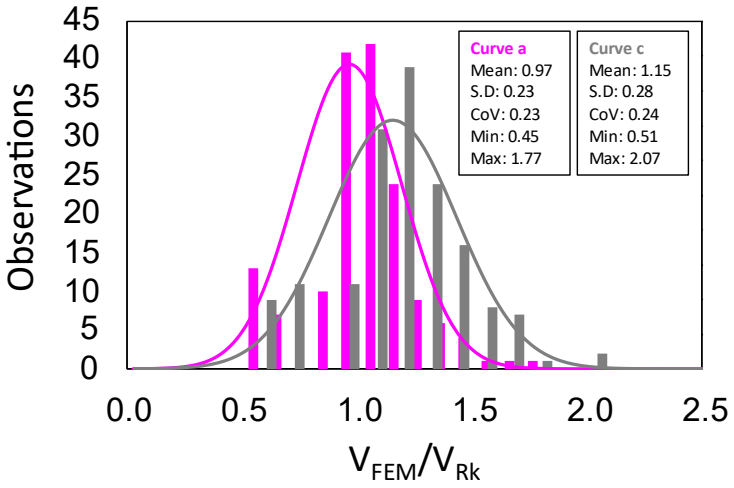

311

312 Fig. 25: Normal distribution

313 To assess the accuracy of the proposed model, both with respect to curves 'a' and 'c', the Mean
314 Absolute Error (MAE) and Root Mean Square Error (RMSE) were calculated using Eqs. (7-8),
315 in which t_i and O_i are the actual and predicted WPB resistance, and N is the total number of
316 data points. Taking into account the proposed procedure applied to buckling curve 'c', the MAE
317 and RMSE were determined to be 80.1 kN and 65.2 kN, respectively. In contrast, buckling
318 curve a demonstrated superior performance, with an MAE of 48.8 kN and an RMSE of 66.5
319 kN. These results clearly indicate that the proposed procedure paired with buckling curve 'a'
320 provides a more accurate prediction of the WPB resistance of composite beams with
321 elliptically-based web openings, highlighting its effectiveness in reducing prediction errors
322 compared to buckling curve 'c'. Vitaliy et al. [13] recently demonstrated that buckling curve

323 'a' provided more accurate WPB resistance predictions than buckling curve 'c', according to
324 the findings of the present study.

$$MAE = \frac{1}{N}\sum_{i=1}^{N}|O_i - t_i| \tag{7}$$

$$RMSE = \sqrt{\frac{\sum_{i=1}^{N}(O_i - t_i)^2}{N}} \tag{8}$$

325

326 5.3.2. Parameter influence

327 Fig. 26 shows the analysis of GCCB1, GCCB2, and GCCB3 models highlighting the impact of
328 geometric parameters of elliptically-based web openings on global shear force and failure
329 modes (i.e., WPB or VM). For GCCB1 and GCCB2 models, at R/d_o = 0.10 and 0.15 (Fig. 26a-
330 26b) with w/d_o = 0.35, the opening width significantly affected global shear, with the GCCB2
331 model showing higher values. At w/d_o = 0.45, the GCCB2 failure mode changed from WPB to
332 VM. Additionally, for R/d_o = 0.25 to 0.30 (Fig. 26c-26e) GCCB2 consistently exhibited higher
333 global shear than the other models. In contrast, GCCB3 models consistently exhibit lower
334 global shear values at a practical range of d_o/H = 0.80, regardless of the opening radius, due to
335 the influence of longer spans, where bending-induced mechanisms outweigh shear effects.

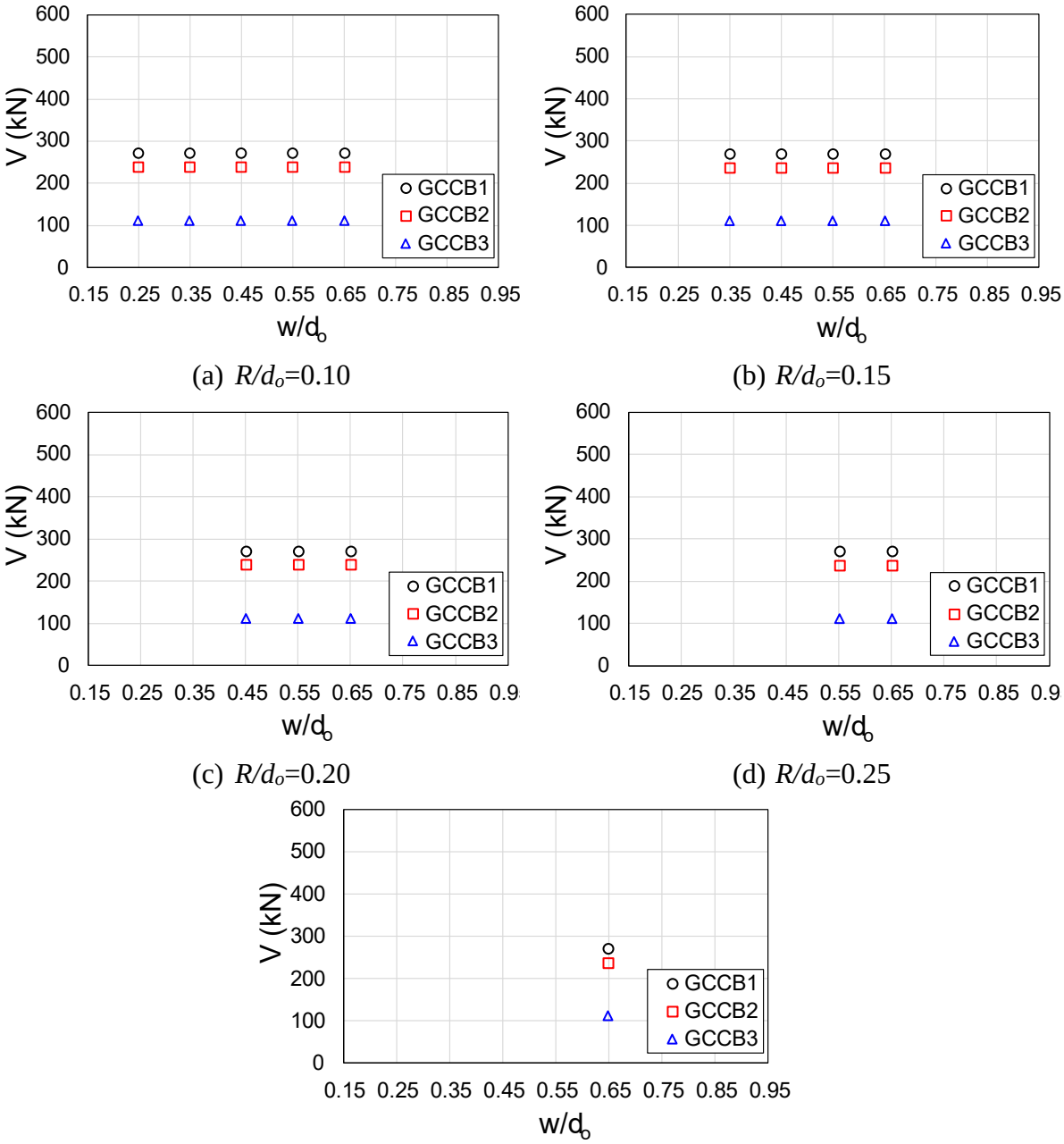

(a) R/d_o=0.10 (b) R/d_o=0.15

(c) R/d_o=0.20 (d) R/d_o=0.25

(e) R/d_o=0.30

336 Fig. 26: Comparison of parameters w/d_o and R/d_o for GCCB1, GCCB2 and GCCB3 models
337 (d_o/H=0.80).

338

339 Fig. 27 illustrates the impact of b_w/d_o ratios on global shear. GCCB3 models consistently
340 displayed lower global shear values than GCCB1 and GCCB2 models, regardless of web-post
341 width. For GCCB1 and GCCB2 models, at *w/do* ratios between 0.25 and 0.35 (Fig. 27a-b),

342 GCCB1 showed higher global shear forces. However, at *w/do* = 0.45, the influence of opening
343 width became more pronounced, resulting in higher global shear in the GCCB2 model (Fig.
344 27c-e), consistent with the earlier observed shift in its failure mode.

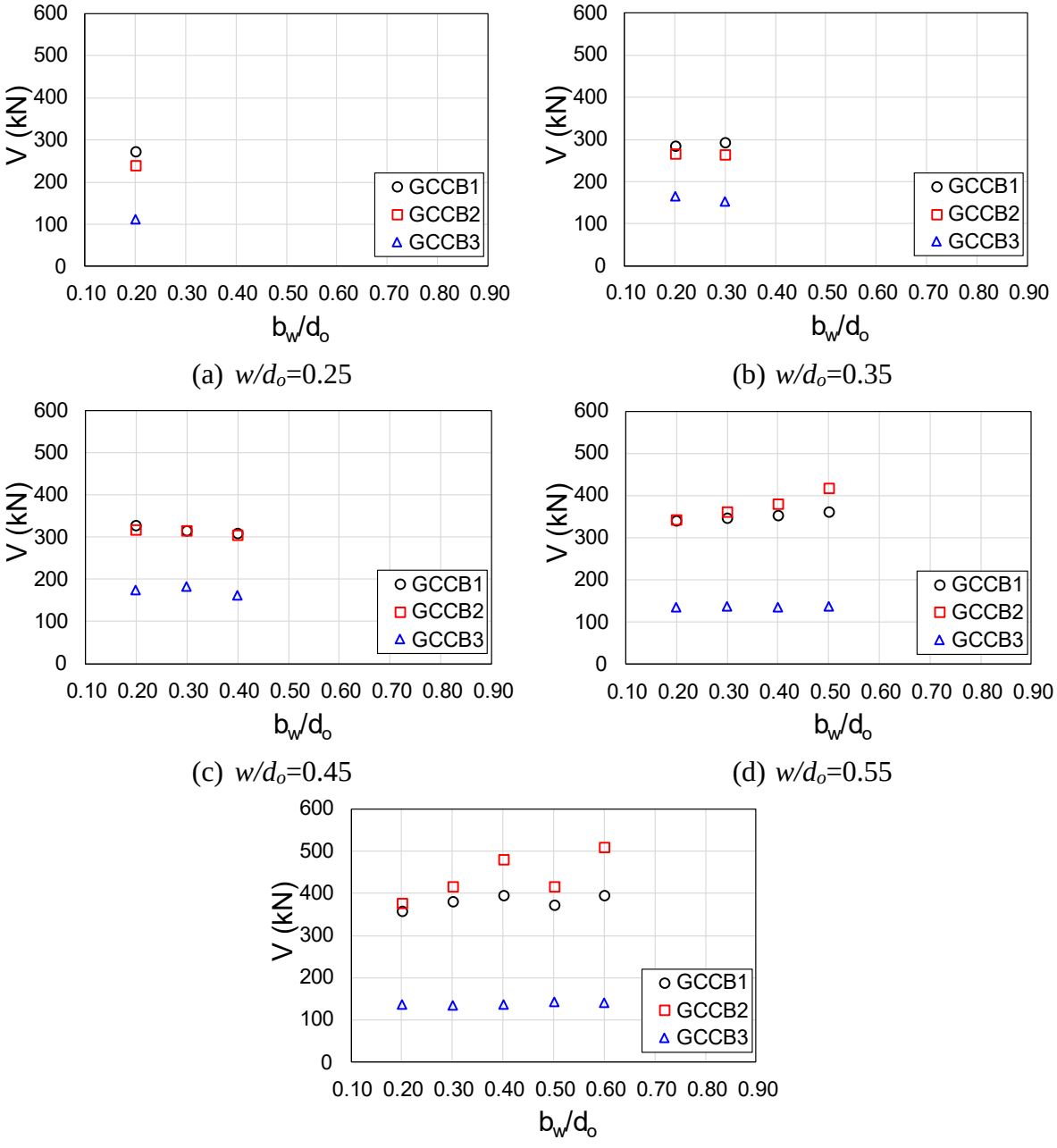

(a) w/d_o=0.25 (b) w/d_o=0.35

(c) w/d_o=0.45 (d) w/d_o=0.55

(e) w/d_o=0.65

345 Fig. 27: Comparison of parameters b_w/d_o and w/d_o for GCCB1, GCCB2 and GCCB3 models
346 (d_o/H=0.80).

The Pearson correlation, as defined in Eq. (9), which quantifies the linear relationship between numerical variables, was calculated, in which, r represents the correlation coefficient, x_i and y_i are the individual values of the variables, and $\bar{x}$ and $\bar{y}$ are their respective means. r = 1 or r = -1 indicates a perfect positive or negative linear correlation, respectively, while r = 0 signifies no linear correlation.

$$r = \frac{\sum(x_i - \bar{x})\,(y_i - \bar{y})}{\sqrt{\sum(x_i - \bar{x})^2 (y_i - \bar{y})^2}} \tag{9}$$

The analysis presented herein includes all models that failed due to WPB, as detailed in Table 2. Fig. 28 illustrates the results. As shown, the parameter w/d_o exhibits the strongest correlation, indicating that variations in w/d_o significantly influence the global shear. Conversely, the parameter d_o/H demonstrates the weakest linear correlation, suggesting that changes in d_o/H have minimal impact on the global shear.

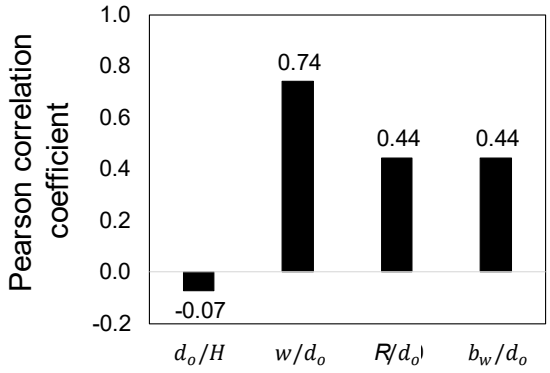

Fig. 28: Comparison of parameters b_w/d_o and w/d_o for GCCB1, GCCB2 and GCCB3 models (d_o/H=0.80).

Conclusions

This paper examines the web-post buckling resistance of steel-concrete composite beams with elliptically-based web openings for the first time, while it has been confirmed previously that perforated beams with large elliptically-based web openings are more susceptible to web-post buckling than Vierendeel bending failure modes. Following the validation study, three models of composite beams were used as reference and parametrically studied; A1 and B1 tests from Nadjai et al. [21] and RWTH 1A test from Müller et al. [22]. A1, B1, RWTH 1A are named here as GCCB1, GCCB2 and GCCB3 models, respectively. The effect of key geometric parameters was examined. The finite element results were compared with an proposed model proposed by Ferreira et al. [3], which considers the buckling curve ‘c’, based on BS EN 1993-1-1 [10]. Also, the results were compared using the same procedure, however, considering the buckling curve 'a', according to the recently published specifications of BS EN 1993-1-13 [12].

The GCCB1 and GCCB2 models failed due to web-post buckling, while GCCB3 failed primarily due to plasticisation from Vierendeel bending. GGCB1 and GGCB2 showed higher V/M ratios (8.42), indicating failure driven by global shear, while GGCB3 had a lower V/M ratio (5.44), reflecting bending-dominated failure. Models with larger web-post dimensions exhibited greater resistance compared to those with smaller web-posts. Resistance increased with larger radius (R) and opening width (w) while maintaining constant opening height (d_o). The impact of the end-post on the resistance of composite beams with elliptically-based web openings was also investigated, considering the variation of the end-post width as function of the web-post width (s-w), with ratios of (s-w)/d_o that ranged from 0.2 to 0.6 in steps of 0.1. The models with larger end-post widths achieved higher resistances.

The model proposed by Ferreira et al. [3] combined with the buckling curve 'c', proved to be a more effective method for predicting web-post buckling in composite beams with elliptically-

based web openings compared to BS EN 1993-1-13 [12] which recommends buckling curve 'a'. Overall, the global shear forces calculated from the numerical models aligned more closely with those estimated by the proposed model, particularly in cases where d_o/H and w/d_o ratios were small. However, as the span increased, the relative error between the numerical and proposed models also increased, changing the failure mode from web-post buckling to plasticisation due to Vierendeel bending.

Acknowledgments

This study was financed in part by the Centro Nacional de Desenvolvimento Cientifico e Tecnológico (CNPq), grant number #404719/2023-6, and the Coordenação de Aperfeiçoamento de Pessoal de Nível Superior – Brasil (CAPES) – Finance Code 001.

References

[1] K.D. Tsavdaridis, C. D'Mello, Optimisation of novel elliptically-based web opening shapes of perforated steel beams, J Constr Steel Res 76 (2012) 39–53. https://doi.org/10.1016/j.jcsr.2012.03.026.

[2] F.P.V. Ferreira, C.H. Martins, S. De Nardin, Advances in composite beams with web openings and composite cellular beams, J Constr Steel Res 172 (2020) 106182. https://doi.org/10.1016/j.jcsr.2020.106182.

[3] F.P.V. Ferreira, R. Shamass, L.F.P. Santos, V. Limbachiya, K.D. Tsavdaridis, EC3 design of web-post buckling resistance for perforated steel beams with elliptically-based web openings, Thin-Walled Structures 175 (2022) 109196. https://doi.org/10.1016/j.tws.2022.109196.

410 [4] R.M.M. Lawson, J. Lim, S.J.J. Hicks, W.I.I. Simms, Design of composite asymmetric
411 cellular beams and beams with large web openings, J Constr Steel Res 62 (2006) 614–
412 629. https://doi.org/10.1016/j.jcsr.2005.09.012.

413 [5] P. Panedpojaman, W. Sae-Long, T. Chub-Uppakarn, Cellular beam design for resistance
414 to inelastic lateral-torsional buckling, Thin-Walled Structures 99 (2016) 182–194.
415 https://doi.org/10.1016/j.tws.2015.08.026.

416 [6] E. Ellobody, Nonlinear analysis of cellular steel beams under combined buckling modes,
417 Thin-Walled Structures 52 (2012) 66–79. https://doi.org/10.1016/j.tws.2011.12.009.

418 [7] K.M. El-Sawy, A.M.I. Sweedan, M.I. Martini, Moment gradient factor of cellular steel
419 beams under inelastic flexure, J Constr Steel Res 98 (2014) 20–34.
420 https://doi.org/10.1016/j.jcsr.2014.02.007.

421 [8] V. V. Degtyarev, S.J. Hicks, F.P.V. Ferreira, K.D. Tsavdaridis, Probabilistic resistance
422 predictions of laterally restrained cellular steel beams by natural gradient boosting, Thin-
423 Walled Structures 205 (2024) 112367. https://doi.org/10.1016/j.tws.2024.112367.

424 [9] K.D. Tsavdaridis, C. D'Mello, Web buckling study of the behaviour and strength of
425 perforated steel beams with different novel web opening shapes, J Constr Steel Res 67
426 (2011) 1605–1620. https://doi.org/10.1016/j.jcsr.2011.04.004.

427 [10] European Committee for Standardization, EN 1993-1-1: Eurocode 3 – Design of steel
428 structures – Part 1-1: General rules and rules for buildings, (2022).

429 [11] R.M. Lawson, S.J. Hicks, Design of composite beams with large web openings, P355
430 ed., The Steel Construction Institute, London, 2011.

[12] European Committee for Standardization, prEN 1993-1-13: Eurocode 3 - Design of steel structures - Part 1-13: Beams with large web openings. Final document, Brussels, (2024).

[13] V. V. Degtyarev, S.J. Hicks, F.P.V. Ferreira, K.D. Tsavdaridis, Design provision assessment for the resistance of laterally restrained cellular steel beams, J Constr Steel Res 226 (2025) 109254. https://doi.org/10.1016/j.jcsr.2024.109254.

[14] R. Shamass, F.P.V. Ferreira, V. Limbachiya, L.F.P. Santos, K.D. Tsavdaridis, Web-post buckling prediction resistance of steel beams with elliptically-based web openings using Artificial Neural Networks (ANN), Thin-Walled Structures 180 (2022) 109959. https://doi.org/10.1016/j.tws.2022.109959.

[15] F.P.V. Ferreira, R. Shamass, L.F.P. Santos, K.D. Tsavdaridis, V. Limbachiya, Web-post buckling resistance calculation of perforated high-strength steel beams with elliptically-based web openings for EC3, Structures 55 (2023) 245–262. https://doi.org/10.1016/j.istruc.2023.05.139.

[16] Sameer S. Fares, J. Coulson, David W. Dinehart, Castellated and Cellular Beam Design 31, American Institute of Steel Construction (2016).

[17] American Institute of Steel Construction, ANSI/AISC 360-16 - Specification for structural steel buildings., (2016).

[18] European committee for standardization, EN 1993-1-1: Eurocode 3 – Design of steel structures – Part 1-1: General rules and rules for buildings, (2002).

[19] European Committee for Standardization, EN 1994-1-1: Eurocode 4 – Design of composite steel and concrete structures – Part 1-1: General rules for buildings., (2004).

452 [20] D. Kerdal, D.A. Nethercot, Failure modes for castellated beams, J Constr Steel Res 4
453 (1984) 295–315. https://doi.org/10.1016/0143-974X(84)90004-X.

454 [21] A. Nadjai, O. Vassart, F. Ali, D. Talamona, A. Allam, M. Hawes, Performance of cellular
455 composite floor beams at elevated temperatures, Fire Saf J 42 (2007) 489–497.
456 https://doi.org/10.1016/j.firesaf.2007.05.001.

457 [22] C. Müller, O. Hechler, A. Bureau, D. Bitar, D. Joyeux, L.G. Cajot, T. Demarco, R.M.
458 Lawson, S. Hicks, P. Devine, O. Lagerqvist, E. Hedman-Pétursson, E. Unosson, M.
459 Feldmann, Large web openings for service integration in composite floors. Technical
460 Steel Research. European Comission, Contract No 7210-PR/315. Final report, (2006).

461 [23] F.P.V. Ferreira, K.D. Tsavdaridis, C.H. Martins, S. De Nardin, Buckling and post-
462 buckling analyses of composite cellular beams, Compos Struct 262 (2021).
463 https://doi.org/10.1016/j.compstruct.2021.113616.

464 [24] F.P.V. Ferreira, C.H. Martins, S. De Nardin, Sensitivity Analysis of Composite Cellular
465 Beams to Constitutive Material Models and Concrete Fracture, International Journal of
466 Structural Stability and Dynamics 21 (2021) 2150008.
467 https://doi.org/10.1142/S0219455421500085.

468 [25] F.P.V. Ferreira, C.H. Martins, S. De Nardin, Assessment of web post buckling resistance
469 in steel-concrete composite cellular beams, Thin-Walled Structures 158 (2021) 106969.
470 https://doi.org/10.1016/j.tws.2020.106969.

471 [26] Dassault Systèmes Simulia, Abaqus 6.18, (2016).

472 [27] R. Shamass, F.P.V. Ferreira, V. Limbachiya, L.F.P. Santos, K.D. Tsavdaridis, Web-post
473 buckling prediction resistance of steel beams with elliptically-based web openings using

474 Artificial Neural Networks (ANN), Thin-Walled Structures 180 (2022) 109959.
475 https://doi.org/10.1016/j.tws.2022.109959.

476 [28] P. Panedpojaman, W. Sae-Long, T. Chub-uppakarn, Cellular beam design for resistance
477 to inelastic lateral–torsional buckling, Thin-Walled Structures 99 (2016) 182–194.
478 https://doi.org/10.1016/j.tws.2015.08.026.

479 [29] Lawson R.M., Oshatogbe D., Newman G.M., Design of FABSEC cellular beams in non-
480 composite and composite applications for both normal temperature and fire engineering
481 conditions. Cellular Beam Software: FBeam 2006 design guide, Fabsec Limited
482 Publication (2006).

483 [30] X. Yun, L. Gardner, Stress-strain curves for hot-rolled steels, J Constr Steel Res 133
484 (2017) 36–46. https://doi.org/10.1016/j.jcsr.2017.01.024.

485 [31] D.L. de L. Araújo, M.W.R. Sales, S.M. de Paulo, A.L.H.C. de C. El Debs, Headed steel
486 stud connectors for composite steel beams with precast hollow-core slabs with structural
487 topping, Eng Struct 107 (2016) 135–150.
488 https://doi.org/10.1016/j.engstruct.2015.10.050.

489 [32] A. Hillerborg, M. Modéer, P.-E. Petersson, Analysis of crack formation and crack growth
490 in concrete by means of fracture mechanics and finite elements, Cem Concr Res 6 (1976)
491 773–781. https://doi.org/10.1016/0008-8846(76)90007-7.

492 [33] J. Lubliner, J. Oliver, S. Oller, E. Oñate, A plastic-damage model for concrete, Int J
493 Solids Struct 25 (1989) 299–326. https://doi.org/10.1016/0020-7683(89)90050-4.

494 [34] J. Lee, G.L. Fenves, Plastic-Damage Model for Cyclic Loading of Concrete Structures,
495 J Eng Mech 124 (1998) 892–900. https://doi.org/10.1061/(ASCE)0733-
496 9399(1998)124:8(892).

497 [35] fib, fib Model Code for Concrete Structures 2010, Wiley-VCH Verlag GmbH & Co.
498 KGaA, Weinheim, Germany, 2013. https://doi.org/10.1002/9783433604090.

499 [36] H.A.W. Cornelissen, D.A. Hordijk, H.W. Reinhardt, Experimental determination of
500 crack softening characteristics of normalweight and lightweight concrete, HERON 31
501 (1986) 1–12.

502 [37] F.P.V. Ferreira, C.H. Martins, S. De Nardin, A parametric study of steel-concrete
503 composite beams with hollow core slabs and concrete topping, Structures 28 (2020) 276–
504 296. https://doi.org/10.1016/j.istruc.2020.08.045.

505 [38] F.P.V. Ferreira, K.D. Tsavdaridis, C.H. Martins, S. De Nardin, Composite action on
506 web-post buckling shear resistance of composite cellular beams with PCHCS and
507 PCHCSCT, Eng Struct 246 (2021) 113065.
508 https://doi.org/10.1016/j.engstruct.2021.113065.

509 [39] M.A. Crisfield, A fast incremental/iterative solution procedure that handles “snap-
510 through,” Comput Struct 13 (1981) 55–62. https://doi.org/10.1016/0045-
511 7949(81)90108-5.

512 [40] M.A. Crisfield, Snap-through and snap-back response in concrete structures and the
513 dangers of under-integration, Int J Numer Methods Eng 22 (1986) 751–767.
514 https://doi.org/10.1002/nme.1620220314.

[41] F.P.V. Ferreira, K.D. Tsavdaridis, C.H. Martins, S. De Nardin, Steel–Concrete-Composite Beams with Precast Hollow-Core Slabs: A Sustainable Solution, Sustainability 13 (2021) 4230. https://doi.org/10.3390/su13084230.

[42] F.P.V. Ferreira, K.D. Tsavdaridis, C.H. Martins, S. De Nardin, Ultimate strength prediction of steel–concrete composite cellular beams with PCHCS, Eng Struct 236 (2021) 112082. https://doi.org/10.1016/j.engstruct.2021.112082.

[43] S.E. Pereira Júnior, F.P.V. Ferreira, K.D. Tsavdaridis, S. De Nardin, Flexural behavior of steel–concrete ultra-shallow floor beams (USFBs) with precast hollow-core slab, Eng Struct 278 (2023) 115524. https://doi.org/10.1016/j.engstruct.2022.115524.

[44] U. Katwal, Z. Tao, M.K. Hassan, Finite element modelling of steel-concrete composite beams with profiled steel sheeting, J Constr Steel Res 146 (2018) 1–15. https://doi.org/10.1016/j.jcsr.2018.03.011.

[45] F.P.V. Ferreira, S.-H. Jeong, E. Mansouri, R. Shamass, K.D. Tsavdaridis, C.H. Martins, S. De Nardin, Five Machine Learning Models Predicting the Global Shear Capacity of Composite Cellular Beams with Hollow-Core Units, Buildings 14 (2024) 2256. https://doi.org/10.3390/buildings14072256.

[46] European Committee for Standardization, prEN 1993-1-14: Eurocode 3 – Design of steel structures – Part 1-14: Design assisted by finite element analysis. Brussels, Belgium, 2023., (2023).

[47] S. Bake Mohamadi, Behaviour of cellular beams and cellular composite floors at ambient and elevated temperatures, PhD, The University of Manchester, 2010.

536 [48] F.P.V. Ferreira, R. Shamass, K.D. Tsavdaridis, Database of Finite Element Method
537 Predictions for Web-Post Buckling Resistance of Steel Beams with Elliptically-Based
538 Web Openings, Mendeley Data 1 (2024). https://doi.org/10.17632/wdnyz9jy8k.1.

539 [49] O. Zhao, L. Gardner, B. Young, Structural performance of stainless steel circular hollow
540 sections under combined axial load and bending – Part 2: Parametric studies and design,
541 Thin-Walled Structures 101 (2016) 240–248. https://doi.org/10.1016/j.tws.2015.12.005.

542